bioRxiv preprint doi: https://doi.org/10.1101/2022.01.19.476895; this version posted February 24, 2022. The copyright holder for this preprint (which was not certified by peer review) is the author/funder, who has granted bioRxiv a license to display the preprint in perpetuity. It is made available under aCC-BY-NC-ND 4.0 International license.

Probing the proton release by Photosystem II in the S₁ to S₂ high-spin transition.

Alain Boussac[1*], Miwa Sugiura[2], Julien Sellés[3]

[1] I²BC, UMR CNRS 9198, CEA Saclay, 91191 Gif-sur-Yvette, France.

[2] Proteo-Science Research Center, and Department of Chemistry, Graduate School of Science and Technology, Ehime University, Bunkyo-cho, Matsuyama, Ehime 790-8577, Japan.

[3] Institut de Biologie Physico-Chimique, UMR CNRS 7141 and Sorbonne Université, 13 rue Pierre et Marie Curie, 75005 Paris, France.

*Corresponding authors: alain.boussac@cea.fr

The authors declare that they have no conflict of interest.

ORCID numbers:

Alain Boussac: 0000-0002-3441-3861

Julien Sellés: 0000-0001-9262-8257

Abbreviations:

Chl, chlorophyll; Chl_{D1}/Chl_{D2}, accessory Chl's on the D1 or D2 side, respectively; PSII, Photosystem II; MES, 2–(*N*–morpholino) ethanesulfonic acid; HEPES, 4-(2-hydroxyethyl)-1-piperazine ethane sulfonic acid. P_{680}, primary electron donor; P_{D1} and P_{D2}; Chl monomer of P_{680} on the D1 or D2 side, respectively, Phe_{D1} and Phe_{D2}, pheophytin on the D1 or D2 side, respectively; Q_A, primary quinone acceptor; Q_B, secondary quinone acceptor; Tyr_Z, redox active tyrosine 161 of D1; WT*3, *T. elongatus* mutant strain containing only the *psbA₃* gene and a His_6-tag on the C-terminus of CP43. EPR, Electron Paramagnetic Resonance spectroscopy; EDNMR, ELDOR-detected Nuclear Magnetic Resonance; ELDOR, Electron-Electron Double Resonance; SQR, sum of the squares of the residues.

Abstract

The stoichiometry and kinetics of the proton release were investigated during each transition of the S-state cycle in Photosystem II (PSII) from *Thermosynechococcus elongatus* containing either a Mn_4CaO_5 (PSII/Ca) or a Mn_4SrO_5 (PSII/Sr) cluster. The measurements were done at pH 6.0 and pH 7.0 knowing that, in PSII/Ca at pH 6.0 and pH 7.0 and in PSII/Sr at pH 6.0, the flash-induced S_2-state is in a low-spin configuration (S_2^{LS}) whereas in PSII/Sr at pH 7.0, the S_2-state is in a high-spin configuration (S_2^{HS}) in half of the centers. Two measurements were done; the time-resolved flash dependent *i*) absorption of either bromocresol purple at pH 6.0 or neutral red at pH 7.0 and *ii*) electrochromism in the Soret band of P_{D1} at 440 nm. The fittings of the oscillations with a period of four indicate that one proton is released in the S_1 to S_2^{HS} transition in PSII/Sr at pH 7.0. It has previously been suggested that the proton released in the S_2^{LS} to S_3 transition would be released in a $S_2^{LS}Tyr_Z{}^\bullet \rightarrow S_2^{HS}Tyr_Z{}^\bullet$ transition before the electron transfer from the cluster to $Tyr_Z{}^\bullet$ occurs. The release of a proton in the $S_1Tyr_Z{}^\bullet \rightarrow S_2^{HS}Tyr_Z$ transition would logically imply that this proton release is missing in the $S_2^{HS}Tyr_Z{}^\bullet$ to S_3Tyr_Z transition. Instead, the proton release in the S_1 to S_2^{HS} transition in PSII/Sr at pH 7.0 was mainly done at the expense of the proton release in the S_3 to S_0 and S_0 to S_1 transitions. However, at pH 7.0, the electrochromism of P_{D1} seems larger in PSII/Sr when compared to PSII/Ca in the S_3 state. This points to the complex link between proton movements in and immediately around the Mn_4 cluster and the mechanism leading to the release of protons into the bulk.

Introduction

Oxygenic photosynthesis is responsible for most of the energy input on Earth by converting the solar energy into fibers, foods and fuels. This process occurs in cyanobacteria, algae and plants. Photosystem II (PSII), the water-splitting enzyme, is at the heart of this process; see for example [1] for a recent view with an evolutionary perspective.

Mature PSII generally consists of 20 subunits with 17 trans-membrane and 3 extrinsic membrane proteins. The PSII binds 35 chlorophylls a (Chl-a), 2 pheophytins (Phe), 1 membrane b-type cytochrome, 1 extrinsic c-type cytochrome (in cyanobacteria and red algae), 1 non-heme iron, 2 plastoquinones (Q_A and Q_B), the Mn_4CaO_5 cluster, 2 Cl^-, 12 carotenoids and 25 lipids [2,3]. Recently, the 4th extrinsic PsbQ subunit has also been found in PSII from *Synechocystis* sp. PCC 6803 in addition to PsbV, PsbO and PsbU [4].

Among the 35 Chls, 31 are antenna Chls and 4 (P_{D1}, P_{D2}, Chl_{D1} and Chl_{D2}) together with the 2 Phe molecules constitute the reaction center of PSII. After the absorption of a photon by the antenna, the excitation energy is transferred to the photochemical trap that consists of the four Chls; P_{D1}, P_{D2}, Chl_{D1}, Chl_{D2}. After a few picoseconds, a charge separation occurs resulting ultimately in the formation of the $Chl_{D1}^+Phe_{D1}^-$ and then $P_{D1}^+Phe_{D1}^-$ radical pair states [5,6].

After the charge separation, P_{D1}^+ oxidizes Tyr_Z, the Tyr161 of the D1 polypeptide, which then is reduced by the Mn_4CaO_5 cluster, see [7] for one recent review. The electron on Phe_{D1}^- is then transferred to Q_A, the primary quinone electron acceptor, and then to Q_B, the second quinone electron acceptor. Whereas Q_A can be only singly reduced under normal conditions, Q_B accepts two electrons and two protons before to leave its binding site and to be replaced by an oxidized Q_B molecule from the membrane plastoquinone pool, [8-11] and references therein.

The Mn_4CaO_5 cluster, oxidized by the $Tyr_Z^\bullet$ radical after each charge separation, cycles through five redox states denoted S_n, where n stands for the number of stored oxidizing equivalents. The S_1-state is stable in the dark and therefore S_1 is the preponderant state upon dark-adaptation. When the S_4-state is formed after the 3rd flash of light given on dark-adapted PSII, two water molecules bound to the cluster are oxidized, O_2 is released and the S_0-state is reformed, [12,13].

Thanks to the advent of serial femtosecond X-ray free electron laser crystallography, structures of the Mn_4CaO_5 cluster have been resolved in the dark-adapted state with the 4 Mn ions in a redox state as close as possible to that in the S_1 state, *i.e.* $Mn^{III}_2Mn^{IV}_2$ [3,14]. The Mn_4CaO_5 structure resemble a distorted chair including a μ-oxo-bridged cuboidal Mn_3O_4Ca

unit with a fourth Mn attached to this core structure *via* two μ-oxo bridges involving the two oxygen's O4 and O5. After further refinement of the electron density maps, some works could indicate an heterogeneity in the valence of Mn ions between the two PSII monomers and/or could show a lower than expected oxidation state of some Mn ions [15-17]. However, other groups [18-20] do not share such a conclusion mainly by taking into account the Jahn–Teller effect on the orientation of the bondings of the Mn^{III}.

Recently, important progresses have been done in the resolution of the crystal structures in the S_2 and S_3 states [21-24]. The structural changes identified in the S_1 to S_2 transition and to a greater extent in the S_2 to S_3 transition are too numerous to detail them in a few lines. Very briefly, these works show that, in S_2, the changes in the structure of the cluster are minor and more or less correspond to those expected for the valence change of the Mn4 from +III to +IV in the context of the high-valence option [18]. Importantly, water molecules in the "O1" and "O4" channels, defined as such because they start from the O1 and O4 oxygens of the cluster, appeared localized slightly differently in S_2 than in S_1. In contrast, in the S_2 to S_3 transition, major structural changes have been detected together with the insertion of a 6th oxygen (O6 or Ox), possibly W3 originally bound to the Ca site, bridging Mn1 and Ca. This oxygen is supposed to correspond to the second water substrate molecule and is close to the bridging oxygen O5 supposed to be the first water substrate molecule [25]. An important movement of the Glu189 residue would allow its carboxylate chain to make a hydrogen bond with the protonated form of this 6th oxygen in S_3 [21].

EPR data studies, supported by computational works, show the existence of more than one structural forms of S_1, S_2 and S_3. The two S_1 EPR signals seen with a parallel mode detection at $g \sim 4.8$ and $g \sim 12$ [26-28] were recently attributed to an orientational Jahn–Teller isomerism of the dangler Mn4 with the valence +III [20]. The authors in [20] further suggested that this isomerism in the S_1 state is at the origin of the valence isomerism in the S_2-state. Indeed, depending on the conditions, at least two S_2 EPR signals can be detected at helium temperatures. The first one has a low-spin $S = 1/2$ value, S_2^{LS}, characterized by a multiline signal made up of at least 20 lines separated by approximately 80 gauss, centered at $g \sim 2.0$ and spread over roughly 1800 gauss [29-31]. The second configuration of S_2 is a high-spin ground state, S_2^{HS}, with $S \geq 5/2$. In plant PSII, S_2^{HS} may exhibit either a derivative-like EPR signal centered at $g \sim 4.1$ [32,33] or more complex signals at higher g values [34,35]. In cyanobacterial PSII, the S_2^{HS} EPR signal has a derivative-like EPR signal centered at $g \sim 4.8$ [36,37].

In a computational work [38], it was proposed that the $g \sim 4.1$ signal in plant PSII have almost the same coordination and environment as the $g \sim 2.0$ signal but with the Mn^{III} ion

located on the dangler Mn4 in the S_2^{HS} state instead on the Mn1 in the S_2^{LS} state. This valence swap would be accompanied by a moving of the oxygen O5 from a position where it links the Mn4, Mn3 and the Ca in the S_2^{LS} configuration to a position where it bridges the Mn1, Mn3 and Ca ions in the S_2^{HS} configuration resulting into the so called closed cubane structure. In other computational works [39,40] the authors arrived at a very different model in which, starting from the S_2^{LS} configuration, the protonation of O4 would lead to an $S = 5/2$ ground state when W1, one of the two water molecules with W2 bound to the dangler Mn4, is present as an aquo ligand. The further deprotonation of W1 to form a hydroxo ligand would then give rise to an $S = 7/2$ ground state [39,40]. In the same work, it was proposed that the form $S = 7/2$ was probably that needed to progress to S_3. The fact that the closed cubane S_2 structure defined in [41,42] is not necessary to progress to S_3 is in line with some earlier works [43]. Experimentally [36,37], the S_2^{HS} form able to progress to S_3 at low temperatures is the $g \sim 4.8$ form, *i.e.* the $S = 7/2$ form that corresponds to an open cubane structure in [39,40].

From an EPR point of view, the S_3-state also exhibits some heterogeneities. The majority of centers exhibit a spin $S = 3$ ground state [44-46]. In this $S = 3$ configuration, the four Mn ions of the cluster have a Mn^{IV} formal oxidation state with an octahedral ligation sphere in an open cubane structure [46]. In this model, the dangler Mn^{IV} ($S = 3/2$) is antiferromagnetically coupled to the open cubane motif $(Mn^{IV})_3$ with $S = 9/2$. The remaining centers are EPR invisible, *e.g.* [37]. The relationship between the different S_2 and S_3 configurations was recently investigated by EPR spectroscopy [37] and discussed in the context of the structural heterogeneities proposed from computational works [41]. In [41], the high-spin S_2-state was considered to be a closed cubane structure something that needs to be reconsidered in view of the proposals made in [39,40] and because there is less and less structural supports for the closed cubane structure, *e.g.* [22].

A third S_3 configuration with a broadened S_3 signal was identified with EDNMR in the presence of glycerol [47,48] and in PSII/Sr [49]. Although in [47] the authors did not completely rule out the presence of a closed cubane, five-coordinate S_3 form, at the origin of this EPR signal, they favored a perturbation of the coordination environment at Mn4 and/or Mn3 in an open cubane S_3 structure induced by glycerol. With X-and Q-band EPR experiments performed in the S_3-state of plant PSII, both in the perpendicular and parallel modes, a high-spin, $S = 6$, was shown to coexist with the $S = 3$ configuration. This $S = 6$ form was attributed to a form of S_3 without O6/Ox bound and with the Mn^{IV}_3 part of the cluster in ferromagnetic interaction with the unsaturated dangler Mn^{IV} [48]. Nevertheless these two forms of S_3 are not detected by X-band EPR, it seems unlikely that they correspond to the EPR invisible S_3

mentioned above. Indeed, the new S_3 signals described in [47,48] are detectable in the presence of glycerol and methanol, whereas the formation of the $(S_2Tyr_Z^\bullet)$' state upon a near-IR illumination in the centers in S_3 defined as EPR invisible is inhibited in the presence of glycerol (and in the presence of methanol in plant PSII) [50,51]. In cyanobacterial PSII/Sr [49], a proportion of centers exhibited a pulsed W-band field-swept S_3 spectrum much broader than in PSII/Ca. This signal was proposed to be present in centers containing a 5-coordinate Mn ion in centers in which no water binding event takes place during the S_2 to S_3 transition. It was therefore proposed that, in these centers, the oxidation event would precede the water binding. Computational works also suggested heterogeneities in S_3 [52-54] with also a $S = 6$ spin value [54,55].

None of the heterogeneities described above were detected in the crystallographic structures of S_2 and S_3 known to date [21-24]. It is quite possible that some of the structural differences that cause the differences identified in EPR are too small to be detectable given the resolution of the crystallographic data. This at least shows, if it were necessary, that spectroscopy remains an indispensable complement to crystallography.

The EPR data summarized above describes a static view of the trapped configurations. Kinetically, it is well documented that the transition from S_2 to S_3 involved at least two phases. The fastest phase, with a $t_{1/2} \leq 25$ μs, is attributed to a proton transfer/release. This fast phase precedes the electron transfer from S_2 to the $Tyr_Z^\bullet$, which occurs with a $t_{1/2} \leq 300$ μs [56-60], and the binding of O6/Ox to the Mn1, *e.g.* [21]. It was discussed earlier that the fast phase could correspond to the release of a proton in an intermediate step $S_2^{LS}Tyr_Z^\bullet \rightarrow S_2^{HS}Tyr_Z^\bullet$ before the $S_2^{HS}Tyr_Z^\bullet \rightarrow S_3^{S=3}$ transition occurs [36]. The existence of intermediate states in the S_2 to S_3 transition was tracked by following, at room temperature, the structural changes in the S_2 to S_3 transition at time points from 50 μs to 200 ms after the 2nd flash [21]. Although no indication was found for a closed cubane intermediate this says, for the moment, nothing on the spin state of the intermediate forms of S_2 able to progress to S_3. Indeed, we have seen above that the S_2^{HS} may have an open cubane structure, *e.g.* [39,40]. In addition, a transient state, by definition, has a low concentration that makes its detection difficult. In an even more recent work [22], a structural dynamics in the water and proton channels was highlighted during the S_2 to S_3 transition.

The question of the existence of a high spin intermediate state in the S_2 to S_3 transition remains. In particular, it is questionable whether the fast phase observed in this transition corresponds to a proton release/movement associated with the formation of a S_2^{HS} state, as has been suggested [36,60]. If this is correct, we would expect to detect a change in the flash pattern

of the proton release in conditions in which the S_2 $g \sim 4.8$ EPR signal is the flash-induced state. In order to probe this model, we have kinetically followed the flash dependent proton release in PSII/Ca and PSII/Sr at pH 6.0 and 7.0, knowing that at pH 7.0 half of the centers exhibit the S_2^{HS} signal at $g \sim 4.8$ in PSII/Sr in contrast to PSII/Ca. This was done by recording absorption changes of pH-responding dyes, *i.e.* bromocresol purple at pH 6.0 and neutral red at pH 7.0, *e.g.* [61,62]. As a control experiment, changes in the electrostatic environment of P_{D1} undergone upon the reduction/oxidation and deprotonation/protonation reactions of either the Mn_4CaO_5 cluster or the Mn_4SrO_5 cluster were also followed by recording the time-resolved absorption change differences 440 nm-*minus*-424 nm during the S-state cycle, *e.g.* [60,63].

Materials and Methods

The *Thermosynechococcus elongatus* strain used was the *ΔpsbA₁, ΔpsbA₂* deletion mutant, referred to as either WT*3-PSII or PsbA3-PSII [64]. This strain was constructed from the *T. elongatus* 43-H strain that had a His_6-tag on the carboxy terminus of CP43 [65]. The cells were cultivated in the presence of either Ca^{2+} or Sr^{2+} [66]. PSII/Ca and PSII/Sr purifications were achieved with a protocol previously described [67].

Absorption changes measurements were done with a lab-built spectrophotometer [68] slightly modified as previously described [67]. The 440 nm-*minus*-424 nm experiments were performed as previously reported [60]. For that, the samples were diluted in 1 M betaine, 15 mM $CaCl_2$, 15 mM $MgCl_2$, and either 40 mM Mes at pH 6.0 or 40 mM Hepes at pH 7.0. The pH of the two solutions was adjusted with NaOH. The measurements with the dyes were done as previously reported [67,69]. In this case, the samples were diluted in 1 M betaine, 15 mM $CaCl_2$, 15 mM $MgCl_2$, and either 150 µM bromocresol purple, *i.e.* 312 times the concentration of PSII, at pH 6.0 or 40 µM neutral red at pH 7.0, *i.e.* 50 times the concentration of PSII. PSII samples were dark-adapted for $\sim$ 1 h at room temperature (20–22°C) before the addition of 100 µM phenyl *p*–benzoquinone (PPBQ) dissolved in dimethyl sulfoxide and 100 µM ferricyanide. The pH of the stock solutions of ferricyanide (100 mM) was adjusted to either pH 6.0 or pH 7.0 prior to their addition to the samples. The chlorophyll concentration of all the samples was $\sim$ 25 µg of Chl/mL. After the $\Delta I/I$ measurements, the absorption of each diluted batch of samples was precisely controlled to avoid errors due to the dilution of concentrated samples. The $\Delta I/I$ values were then normalized to $A_{673} = 1.75$, that is very close to 25 µg Chl/mL with $\varepsilon \sim 70$ mM^{-1}·cm^{-1} at 674 nm for dimeric PSII [70].

The fittings of the data were done as previously described [60,63,66,71] with the additional details given in the text by using the Excel solver. All the data are the average of 2 to 3 experiments done on different batches of PSII resulting from different purifications. The noise defined as the maximum variation of the averaged signal before the first actinic flash was $\sim \pm 70 \ 10^{-6} \ \Delta I/I$ units at 575 nm, $\sim \pm 30 \ 10^{-6} \ \Delta I/I$ units at 547 nm and $\sim \pm 20 \ 10^{-6} \ \Delta I/I$ units for the 440 nm-*minus*-424 nm difference.

Results

Stoichiometry of the S-state dependent proton release.

After one-flash illumination given at pH 6.0 to dark-adapted PSII, *i.e.* in the S_1-state, both PSII/Ca and PSII/Sr exhibit a $S = 1/2$ low-spin configuration, S_2^{LS} [36] At pH 7.0, the S_2^{LS} state is the flash-induced state in PSII/Ca whereas in PSII/Sr a proportion of centers exhibits a S_2-state in a $S \geq 5/2$ high-spin configuration, S_2^{HS}. In our previous work [36], in which the PSII was first washed in a buffer-free medium and then the pH was directly adjusted in the EPR tubes by adding 100 mM of different buffers, we found that the pK value of the $S_2^{LS} \leftrightarrow S_2^{HS}$ equilibrium was ~ 7.5. However, after this earlier work, we have found that such a protocol overestimated the pH values by ~ 0.5 pH unit so that the pK of the $S_2^{LS} \leftrightarrow S_2^{HS}$ equilibrium is actually ~ 7.0 instead of 7.5. The data at pH 7.0 in PSII/Sr in this work therefore correspond to a situation in which 50 % of the centers are in S_2^{HS} state (and this has been controlled by EPR with PSII/Sr washed with a large volume of the medium at pH 7.0, not shown). It would have been much more comfortable for the interpretation of the results to do the experiment at pH values where the proportion of S_2^{HS} is greater. Unfortunately, for higher pH values than 7.0, the integrity of the PSII/Sr estimated by recording the amplitude of the S_2^{LS} and S_2^{HS} EPR signals after variable times (not shown), and by following the amplitude of the period four oscillations (not shown), decreases much faster than the time required for doing the experiments reported here (about 2 hours and half). This problem did not occurred in previous EPR experiments [36] since in this case the samples were frozen immediately after the addition of the buffers.

Fig. 1, shows the absorbance changes of either bromocresol purple at pH 6.0 (purple full circles in Panels A and B) or neutral red at pH 7.0 (red full circles in Panels C and D). The $\Delta I/I$ were measured 100 ms after each flash, 400 ms apart, of the series. The measurements were done with PSII/Ca in Panels A and C and with PSII/Sr in Panels B and D. A proton released by PSII, *i.e.* an acidification of the bulk, results in a decrease of the absorption at 575 nm with

bromocresol purple and in an increase of the absorption at 547 nm with neutral red. The wavelength of 547 nm was chosen because it corresponds to the isosbestic point of the electrochromic blue shift undergone by Phe_{D1} in the Q_X absorption region upon the formation of Q_A^- with PsbA3 as the D1 protein, *e.g.* [60].

In PSII/Ca, at pH 6.0 (Panel A), there was a large increase in the absorption after the first flash. Since no proton release is supposed to occur in the S_1 to S_2 transition in such a sample at this pH, this change in the $\Delta I/I$ mainly corresponds to a proton uptake coupled to the reduction of the oxidized non-heme iron by Q_A^-. After the 5th flash, the $\Delta I/I$ change remained positive. This clearly indicates that there was also a proton uptake after this 5th flash (mainly the S_1 to S_2 transition during the second turnover). In PSII/Ca at pH 7.0 (Panel C), with neutral red, this absorption due to the proton uptake coupled to the reduction of the oxidized non-heme iron seemed much more pronounced. Indeed, at least until the 21st flash there was a negative contribution of the $\Delta I/I$ after the 3rd and 4th flashes, the 7th and 8th, and so on, flashes. In the analysis of such experiments, the data from the first flash are usually discarded due to several non-oscillating contributions [63]. In previous works, we did not consider that the non-heme iron could contribute after the first flash [67,69,71]. The data in Panel A and C in Fig. 1 show that this is not completely true under the present conditions. Although the conclusions made previously remain valid, the smallness of the effects that are expected here require to take into account the proton uptake coupled to the reduction of the non-heme iron after each flash of the series. To this end, the stoichiometry of the proton release was therefore estimated for different amounts of proton uptake occurring on each flash, assuming that this proton uptake is the same on all flashes from the 2nd onwards. This procedure is more or less equivalent to adding a constant offset to the proton release calculated as described previously [71]. This offset also takes into account the slow drift that was equally present on all flashes. This drift has an unknown origin and may vary from experiment to experiment. Part of this process probably involves the release of a proton due to the reoxidation of non-heme iron during the dark period between flashes.

Fig. 2 shows the results of these fittings at pH 6.0 for PSII/Ca in Panel A and for PSII/Sr in Panel B. Panel C and D shows the fittings at pH 7.0 for PSII/Ca and PSII/Sr, respectively. The X-axis corresponds to the different values of the offset, in $\Delta I/I$ units, which were tested in the fitting procedure. This offset corresponds to the sum of the proton uptake following the reduction of the non-heme iron and the drift 100 ms after the flash. The values h_0 (green curve), h_1 (black curve), h_2 (red curve), h_3 (blue curve) are the fitted $\Delta I/I$ corresponding to the release of proton(s) in the S_0 to S_1, S_1 to S_2, S_2 to S_3 and S_3 to S_0 transitions, respectively, for each

offset value. The yellow curves correspond to the sum of the squares of the residues (SQR) calculated from the 2nd to the 40th flash. At pH 6.0, the SQR was multiplied by -1 for a better visualisation of the curves in the graph.

At pH 6.0, in both PSII/Ca and PSII/Sr, whatever the offset value, there was no proton release in the S_1 to S_2 transition (black curves). For offset values resulting in the smallest SQR, the proton release estimated from the relative amplitudes of the $\Delta I/I$ was similar in the S_2 to S_3 (red curves) and S_0 to S_1 (green curves) transitions and almost twice in the S_3 to S_0 transition (blue curves) as generally found for the pattern of the proton release [61,62].

At pH 7.0, in PSII/Ca, when the SQR was the smallest, the proton release on the S_1 to S_2 transition remained either zero (or very small if not zero). In the S_0 to S_1 transition, the proton release became smaller than in the S_2 to S_3 transition as observed in PSII from plant [62]. In PSII/Sr, at pH 7.0, the proton release in the S_1 to S_2 transition significantly increased to ~ 0.5 and that constitutes the main result of this experiment. These observations will be further discussed with the analysis of the kinetics in Fig. 4. However, we can already note that the larger proton release in the S_1 to S_2 transition in PSII/Sr at pH 7.0 was done in part at the expense of the proton release in the S_3 to S_0 and S_0 to S_1 transitions when compared to the situation in PSII/Ca at pH 7.0. Table 1 summarizes the results of the fittings. The crosses joined by dashed lines in Fig. 1 are the fits using the values reported in Table 1. The sums of the $\Delta I/I$ for an offset of $\sim$ -800 at pH 7.0 are comparable in PSII/Ca and PSII/Sr which shows that the apparent smaller amplitudes of the oscillations at this pH are due to a different stoichiometry of the proton release.

The correspondence between the $\Delta I/I$ values calculated in Table 1 in PSII/Ca at pH 7.0 with neutral red and the number of proton released was also estimated by following the OD changes of this dye at 547 nm with a UV-vis spectrometer (UVIKON-XL) between pH 7.04 and pH 6.95 upon the successive addition aliquots of HCl at 38 mM (not shown). With this procedure, we found that the $\Delta I/I$ value of 3738 10^{-6} found for a full cycle of the enzyme was equivalent to the addition of 3.5 protons into the bulk which is in very good agreement with the value of 3.6 estimated for a miss parameter of 10 %. Although some simplifications in this control potentially decrease the accuracy of the comparison, it gives significant credit to the quantification of the number of protons released by PSII. It also shows that PSII has little or no buffer capacity. That said, if this had been the case, one could not observe the oscillations with a period of 4 with identical parameters from the beginning to the 40th flash.

Flash-dependence of the 440 nm-minus-424 nm electrochromism.

A way to follow the charge(s) in and around the $Mn_4(Ca/Sr)O_5$ cluster is to record the electrochromic band-shifts in the Soret region of the P_{D1} absorption spectrum at 440 nm. This measurement takes into account both the proton uptake/release and the electron transfer events, *e.g.* [60,62] and references therein. For the removal of the contributions due to the reduction of Q_A the $\Delta I/I$ at 424 nm was also measured. Indeed, the electrochromism due to Q_A^- equally contributes at 440 nm and 424 nm [72]. The amplitude of the 440 nm-*minus*-424 nm difference was then plotted. Unlike the situation with the dyes, the electrochromism is not contaminated by the reduction/oxidation of the non-heme iron and the coupled protonation/deprotonation [73,74]. The simulation of the oscillations was therefore done without this contribution as described previously for the oscillations at other wavelengths [63,66].

Fig. 3 shows the 440 nm-*minus*-424 nm differences induced by each flash of a series given on dark-adapted PSII and measured 100 ms after these flashes. Data in Panels A and B were obtained at pH 6.0 and data in Panels C and D at pH 7.0. The samples were PSII/Ca in Panels A and C and PSII/Sr in Panels B and D. The red full circles are the experimental data and the crosses joined by dashed lines are the results of the fitting procedure. Table 1 summarizes the results from the fittings.

At pH 6.0, the oscillations with a period of four were clearly detectable at least until the 40th flash in both PSII/Ca and PSII/Sr. At pH 7.0, although the oscillations persisted at least until the 40th flash in Fig. 1, the oscillations of the electrochromism significantly decreased after the 25th flash in both PSII/Ca and PSII/Sr. In the four cases, the larger electrochromism is detected on the 1st, 5th, 9th and so on, flashes, *i.e.* in the $S_1Tyr_Z^\bullet$ to S_2Tyr_Z transition when the oxidation of the Mn_4 cluster is not, or only partially, compensated by a proton release. In the four samples, after the 2nd flash and the 4th flash, *i.e.* in the $S_2Tyr_Z^\bullet$ to S_3Tyr_Z and $S_0Tyr_Z^\bullet$ to S_1Tyr_Z transitions, the electrochromism is minimum, as expected, since a proton release occurs with the oxidation of the Mn_4 cluster. After the 3rd flash, *i.e.* in $S_3Tyr_Z^\bullet$ to S_0Tyr_Z transition, the electrochromism is negative because the cluster is fully reduced and 1 to 2 protons are released. Nevertheless these similarities, small but significant differences are visible, particularly in PSII/Sr at pH 7.0. Indeed, after the first flash, the amplitude of the absorption change was relatively smaller than in PSII/Ca at pH 7.0. In compensation, after the 2nd flash, the change in the absorption was positive in PSII/Sr and negative in PSII/Ca. These differences either did not exist or were less pronounced at pH 6.0 and it is tempting to explain them by a release of proton in a fraction of the centres in PSII/Sr at pH 7.0 after the 1st flash as suggested by the result of

the experiment reported in Figs. 1 and 2. These observations are further analysed with the kinetics shown in Fig. 5.

Kinetics of the S-state dependent proton release.

Fig. 4 shows the kinetics of the decays of the absorption changes of either *i*) bromocresol purple at pH 6.0 with PSII/Ca (Panel A) and PSII/Sr (Panel B) or *ii*) neutral red at pH 7.0 with PSII/Ca (Panel C) and PSII/Sr (Panel D). The measurements were done after the 1st (black points), the 2nd (red points), the 3rd (blue points) and the 4th (green points) flashes given on dark-adapted PSII. The dashed lines joining are spline curves plotted for a better visualisation of the kinetics.

In PSII/Ca, at pH 6.0 (Panel A in Fig. 4), the kinetics were very similar to those already described at pH 6.3 [67]. After the first flash, the increase in the $\Delta I/I$ with a $t_{1/2}$ close to 300 µs corresponds to the proton uptake following the reduction of the non-heme iron by Q_A^- which occurs with a $t_{1/2} \sim 50$ µs [10]. After the second flash, a proton release occurred with a $t_{1/2}$ close to 60 µs. After the third flash, a biphasic proton release kinetics was resolved. The fastest phase decayed with a $t_{1/2}$ of ~ 40 µs and the slowest one decayed with $t_{1/2} \approx 1$-2 ms. These two phases in the proton release likely corresponds to the two steps in the $S_3 Tyr_Z^\bullet \rightarrow (S_3 Tyr_Z^\bullet)' \rightarrow S_0 Tyr_Z$ transitions, *e.g.* [56,72]. Since the number of protons released in this transition is 1.68 (Table 1) the data can be interpreted with 1 proton released in the first of these two steps and 0.68 in the second one. After the 4th flash, *i.e.* in the $S_0 Tyr_Z^\bullet$ to $S_1 Tyr_Z$ transition, a proton release occurred with a $t_{1/2}$ of ~ 200 µs. This proton release in the $S_0 Tyr_Z^\bullet$ to $S_1 Tyr_Z$ transition is approximately 4 times slower than the oxidation of the Mn_4CaO_5 cluster by $Tyr_Z^\bullet$ [56,60]. For the longest times, the slow drift discussed above is clearly visible. It does not significantly perturbs the interpretation of the kinetics before 1 ms. For example, in this time range, it is clear that the amplitude of the absorption changes are comparable in the $S_2 Tyr_Z^\bullet$ to $S_3 Tyr_Z$, $S_0 Tyr_Z^\bullet$ to $S_1 Tyr_Z$ and $S_3 Tyr_Z^\bullet \rightarrow (S_3 Tyr_Z^\bullet)'$ transitions. However, the drift may slightly decrease the amplitude of the slower phase in the S_3 to S_0 transition. The $\Delta I/I$ changes observed between 5 µs and 10 µs, were likely due electrostatic effects on the dyes [75], as previously discussed [67].

At pH 6.0 (Panel B), the proton uptake after the first flash in PSII/Sr, with a $t_{1/2}$ close to 1 ms, was significantly slower than in PSII/Ca. The proton release in the $(S_3 Tyr_Z^\bullet)' \rightarrow S_0 Tyr_Z$ transition was also slowed down from ~ 1-2 ms to ~ 5 ms in agreement with previous results upon the Ca/Sr exchange [66,71]. In the 3 other transitions, $S_2 Tyr_Z^\bullet \rightarrow S_3 Tyr_Z$, $S_0 Tyr_Z^\bullet \rightarrow$

$S_1 Tyr_Z$ and $S_3 Tyr_Z^\bullet \rightarrow (S_3 Tyr_Z^\bullet)'$, the kinetics of the proton release had similar $t_{1/2}$ in PSII/Sr and PSII/Ca.

At pH 7.0, the proton uptake on the first flash (black points) in PSII/Ca occurred with a $t_{1/2} \leq 200$ µs. This proton uptake occurs over a similar time range as the proton release in the other transitions. For example, after the 3rd flash, *i.e* in the $S_3 Tyr_Z^\bullet \rightarrow (S_3 Tyr_Z^\bullet)' \rightarrow S_0 Tyr_Z$ transitions, a proton uptake was clearly detected after the proton release which occurs in the $S_3 Tyr_Z^\bullet \rightarrow (S_3 Tyr_Z^\bullet)'$ and before the proton release occurring in the $(S_3 Tyr_Z^\bullet)' \rightarrow S_0 Tyr_Z$ transition. Despite this complication, the kinetics in PSII/Ca at pH 7.0 appeared similar to those observed in PSII/Ca at pH 6.0. Table 2 shows an estimate of the $t_{1/2}$ values after each flash. In PSII/Sr, at pH 7.0, the proton uptake on the first flash had a similar rate as in PSII/Ca at pH 7.0 and pH 6.0. Unfortunately, this proton uptake occurring on the first flash makes difficult the detection of the kinetics corresponding to the release of the ~ 0.5 proton.

S state-dependent kinetics of the electrochromism 440 nm-minus-424 nm.

Fig. 5 shows the kinetics of the 440 nm-*minus*-424 nm differences in the four samples. Panels A and B were measured at pH 6.0 and Panels C and D at pH 7.0. The samples were PSII/Ca in Panels A and C and PSII/Sr in Panels B and D. The absorption change differences 440 nm-*minus*-424 nm are shown after the 1st flash (black), the 2nd flash (red), the 3rd flash (blue), and the 4th flash (green) given to dark-adapted samples. The dashed lines joining the data points are spline curves plotted for a better visualisation of the kinetics. Table 2 shows an estimate of the $t_{1/2}$ values after each flash.

After the 1st flash (black points), the 440 nm-*minus*-424 nm difference decayed with a $t_{1/2}$ close to 20-30 µs in PSII/Ca at both pH 6.0 (Panel A) and pH 7.0 (Panel C). This decay corresponds to the electron transfer from the $Mn_4 CaO_5$ cluster to Tyr_Z in the $S_1 Tyr_Z^\bullet$ to $S_2 Tyr_Z$ transition since no proton release into the bulk is involved here. In PSII/Sr at pH 6.0 (Panel B), and pH 7.0 (Panel D), the global $t_{1/2}$ of the decay after the 1st flash was close to 200 µs. However, we cannot discard an additional fast phase with a $t_{1/2}$ close to 20 µs at pH 7.0. The phase with a $t_{1/2} \sim 200$ µs is almost 10 times slower in PSII/Sr than in PSII/Ca. This difference between PSII/Ca and PSII/Sr is slightly larger than that one previously estimated by following the increase of the absorption of the Mn_4 cluster in the UV [66]. In both PSII/Ca and PSII/Sr, the amplitude of the decay is approximately twice at pH 7.0 than at pH 6.0. This could suggest that the electrostatic constraint, that is induced by the formation of $Tyr_Z^\bullet$ in the S_1 state, and that is

relaxed during the electron transfer in the $S_1Tyr_Z^\bullet$ to S_2Tyr_Z transition, is larger at pH 7.0 than as pH 6.0.

After the 2nd flash, two phases were previously identified at pH 6.5 [60]: a fast one with a $t_{1/2} < 20$ μs and a slower one with a $t_{1/2}$ between 100 and 200 μs. The slow phase, much slower than the proton release measured with bromocresol purple, has been proposed to correspond to the electron transfer from the Mn_4 cluster in the S_2 state to $Tyr_Z^\bullet$ and the fast phase to a proton movement around the Mn_4 cluster possibly triggered by the formation of the S_2^{HS} state in the presence of $Tyr_Z^\bullet$. In PSII/Ca at pH 6.0, Panel A in Fig. 5, the decay after the 2nd flash (red points) was qualitatively similar to that one described previously at pH 6.5 [60] with a $t_{1/2}$ for the fast phase close to 10-20 μs. In PSII/Ca at pH 7.0 (Panel B), although less evident, the decay seemed also biphasic with $t_{1/2}$ values close to 20 μs and 200 μs. In PSII/Sr, the kinetics was similar at pH 6.0 (Panel C) and pH 7.0 (Panel D), with the two $t_{1/2}$ values close to 20 μs and 200 μs.

After the 3rd flash (blue points), two phases were detected in all cases. There is a consensus to attribute the fast phase to the $S_3Tyr_Z^\bullet$ to $(S_3Tyr_Z^\bullet)'$ + H^+ transition and the slow one to the $(S_3Tyr_Z^\bullet)'$ to S_0Tyr_Z + H^+ transition. In PSII/Ca, the amplitudes of the fast and slow phases were similar at pH 6.0 (Panel A) and pH 7.0 (Panel C) and the two $t_{1/2}$, ~ 20 μs and ~1 ms, were also similar. In PSII/Sr, the $t_{1/2}$ of the slow phase increased to ~ 5 ms at pH 6.0 (Panel B) and pH 7.0 (Panel D). At pH 7.0, in PSII/Sr, a fast phase with a $t_{1/2}$ ~ 20-30 μs was clearly present. This fast phase seemed to have a smaller amplitude at pH 6.0. The amplitude of the decay of the ΔI/I after the 3rd flash was similar in PSII/Ca and PSII/Sr at pH 7.0. In contrast, at pH 6.0, this amplitude was smaller at pH 6.0 in PSII/Sr than in PSII/Ca.

After the 4th flash, i.e. in the $S_0Tyr_Z^\bullet$ to S_1Tyr_Z transition, in PSII/Ca at pH 6.5, two phases were previously identified and discussed [60]. The fast one with a $t_{1/2}$ ~ 10-20 μs corresponds to the electron transfer and the slow one with a $t_{1/2}$ ~ 200 μs to the proton release. This again confirmed that the electron transfer precedes the proton release in this transition [56,60]. In Fig. 5, the kinetics after the 4th flash (green points) are in full agreement with these conclusions for PSII/Ca at pH 6.0 and pH 7.0. In PSII/Sr at pH 7.0, the slow phase of the 440 nm-minus-424 nm difference with a $t_{1/2}$ ~ 200-300 μs fits well with the kinetics of the proton release in Panel B of Fig. 4. Thus, the electron transfer with a $t_{1/2}$ close to 10-20 μs also precedes the proton release in the $S_0Tyr_Z^\bullet$ to S_1Tyr_Z transition of PSII/Sr at pH 7.0. At pH 6.0, the situation seems to differ in PSII/Sr. Indeed, there is likely only one phase in the 440 nm-minus-424 nm difference decay with a $t_{1/2}$ ~ 500 μs. This kinetics is either similar or slightly

slower than the proton release occurring with a $t_{1/2} \sim 300$ µs, which suggests that at pH 6.0, in PSII/Sr, the proton release is time-coupled to (or slightly precedes) the electron transfer in the $S_0Tyr_Z^{\bullet}$ to S_1Tyr_Z transition.

Discussion

The configuration of the S_2 state capable of progressing to S_3 remains highly debated in the literature, *e.g.* [21,40-42,49,53,55, 76-82]. Experimentally, in PSII from *T. elongatus*, a S_2^{HS}, $S \geq 5/2$ spin state, with a *g* value close to 4.8-4.9 could reach the $S_3^{S=3}$ state upon an illumination at temperatures ≤ 200 K while the multiline $S_2^{S=1/2}$ state could not [36,37]. In these works, the S_2^{HS} state was observed at high pH and it was suggested that increasing the pH would mimic the electrostatic influence of $Tyr_Z^{\bullet}(His^+)$ by displacing the $S_2^{LS} \leftrightarrow S_2^{HS}$ equilibrium to the right as proposed in a computational work [76]. In this model, at normal pH values, the rapidly released proton in the S_2 to S_3 transition before the electron transfer occurs [36,56-60], *i.e.* in the $S_2^{LS}Tyr_Z^{\bullet}(His^+)$ state, was proposed to correspond to the formation of the S_2^{HS} state triggered by $Tyr_Z^{\bullet}(His^+)$ [36]. In such a model, a change in the flash pattern of the proton release is expected when the flash-induced S_2-state is high-spin instead of low-spin. This is what we have been looking for in this work. For that, we have followed the proton release in PSII/Ca and PSII/Sr at pH 6.0 and 7.0, knowing that at in PSII/Ca at pH 6.0 and 7.0 and in PSII/Sr at pH 6.0 there is no flash induced S_2^{HS} state. In contrast, about half of the centers in PSII/Sr exhibit S_2^{HS} signal at $g \sim 4.8$ at pH 7.0. Given the incredible amount of literature describing different sequence of events in the S_2 to S_3 transition, it has become impossible, in a normal article, to discuss all of them and, instead, we have focus our attention on those that we feel are most relevant to the present work. For taking into account some pH dependencies not linked to the formation of a S_2^{HS} state, the data in PSII/Sr at pH 7.0 were compared to those in PSII/Sr at pH 6.0 but also to those in PSII/Ca at pH 7.0 and pH 6.0.

In PSII/Ca at pH 6.0, the flash pattern for the release into the bulk of the 4 protons is 1.20, 0.0, 1.13, 1.68 for the $S_0{\rightarrow}S_1$, $S_1{\rightarrow}S_2$, $S_2{\rightarrow}S_3$, $S_3{\rightarrow}S_0$ transitions, respectively (Table 1). This pattern is comparable, but not identical, to that found in plant PSII at pH 6.0 obtained in a similar experiment that was 1.52, 0.05, 1.0, 1.43 [62]. In [62], the value for the S_3 to S_0 transition was computed as the complement to 4 of the sum of the 3 other transitions. The main difference in plant PSII when compared to PSII from *T. elongatus* is a higher value for the $S_0{\rightarrow}S_1$ transition compensated by a lower value for the $S_3{\rightarrow}S_0$ transition. In the FTIR

conditions, at pH 6.0, the pattern was found to be 0.94, 0.28, 1.20, 1.57 in PSII from *T. elongatus* [83]. In plant PSII at pH 7.0, the flash pattern for the proton release into the bulk was 1.10, 0.32, 1.0, 1.58 [62]. In PSII/Ca from *T. elongatus*, at pH 7.0, a significantly different pattern is found here with 0.77, 0.02, 1.13, 2.08. However, in PSII/Ca from *T. elongatus* and from plant, the number of protons released in the S_2 to S_3 transition is either very weakly or not affected upon increasing the pH value from 6.0 to 7.0. The other similarities between these two PSII observed upon an increase of the pH from 6.0 to 7.0 is a decrease of the number of proton(s) that are released in the S_0 to S_1 transition and an increase of the number of proton(s) that are released in the S_3 to S_0 transition. The important difference is the release of 0.32 proton in the S_1 to S_2 transition in plant PSII whereas in *T. elongatus* the value remains close to 0. This difference is difficult to rationalize because a pH dependence of the S_1 to S_2^{LS} transition between 6.0 and 7.0 in plant PSII was not reported in the literature, *e.g.* [84]. Therefore, it more likely originates from differences in the pK, in S_1 and S_2, of some of the groups in the long distance H-bond networks involved in the egress of protons into the lumen upon the oxidation of the Mn_4CaO_5 cluster that likely involve the extrinsic subunits, which differ between plant and cyanobacteria, *e.g.* [85, 86]. For that reason, it could be better to compare the pH effects in PSII from only one origin, here *T. elongatus*. In addition, there is no study describing the flash pattern for the proton release in PSII/Sr from plant and the properties of the S_2^{HS} state are different in plant PSII from an EPR point of view.

In PSII/Sr from *T. elongatus*, at pH 6.0, the flash pattern is 1.35, 0.0, 1.11, 1.54 for the $S_0{\rightarrow}S_1$, $S_1{\rightarrow}S_2$, $S_2{\rightarrow}S_3$, $S_3{\rightarrow}S_0$ transitions, respectively. These values are very close to those found earlier, at pH 6.3, in PSII/Sr in which Cl^- was replaced with Br^-. Indeed, the pattern was 1.16, 0.02, 1.19, 1.63 [71]. These values are also very close to those found in PSII/Ca which indicates that either the pK values of the groups involved in the proton release are neither affected by the Ca^{2+}/Sr^{2+} exchange nor by the Cl^-/Br^- exchange, or that at pH 6.0 we are far from these pK values. This later possibility would agree with the low (≤ 4.5) and high (≥ 9.5) S-state dependent pK values of 3 of the 4 groups proposed to be involved in the different Sn states that were calculated in [62].

In PSII/Sr at pH 7.0 the number of proton(s) released in the S_1 to S_2 transition increased to 0.47. This increase seems mainly compensated by a decreased in the S_0 to S_1 transition with 1.02 proton at pH 7.0 instead of 1.35 at pH 6.0 when the reference is the PSII/Sr at pH 6.0. However, increasing the pH in PSII/Ca from 6.0 to 7.0 without favoring the formation of S_2^{HS} also increases the number of proton released in the S_0 to S_1 transition so that the step in which there is a missing proton when the S_2^{HS} is formed remains to be identified

with certainty. It should also be noted that in purified plant PSII the increase in the number of protons released in the S_1 to S_2 transition when the pH is increased from 6.0 to 7.0 is not compensated by a decrease in the S_2 to S_3 transition but by a decrease in the S_0 to S_1 transition [62].

The 440 nm-*minus*-424 nm differences take into account the increase/decrease of the electrostatic environment of P_{D1}. In the S-state transitions in which the oxidation of the cluster is preceded/followed by a proton release, the 440 nm-*minus*-424 nm difference is expected to be small. Conversely, the 440 nm-*minus*-424 nm difference is expected to be larger when no proton is released. This is what is observed in PSII/Ca at both pH 6.0 and pH 7.0 and in PSII/Sr at pH 6.0 where no proton are released in the S_1 to S_2 transition. For a same proton pattern, the 440 nm-*minus*-424 nm differences are smaller at pH 6.0 in PSII/Sr than in PSII/Ca. This shows that the change in the H-bond network around the Mn_4 cluster induced by the Ca^{2+}/Sr^{2+} exchange have a global consequence on the electrostatic environment of P_{D1} in the S-state cycle.

In PSII/Sr at pH 7.0, in the S_1 to S_2 transition, the 440 nm-*minus*-424 nm difference is not smaller than at pH 6.0 while 0.47 protons are released. However, whereas in PSII/Ca the ε_1 extinction coefficient at pH 7.0 is 1.37 times the value at pH 6.0, in PSII/Sr the ε_1 extinction coefficient at pH 7.0 is only 1.14 times the value at pH 6.0. This suggests that the electrostatic constraint on P_{D1} differs in the S_2^{HS} and S_2^{LS} states and therefore that the H bond network is different in the two spin states of S_2. Such a result is not surprising since, whatever the structural model for the S_2^{HS} configuration, the distribution of the charges inside and protons inside and around the cluster differs significantly from those in the S_2^{LS} configuration, *e.g.* [40,42,76,77,79]. We also know that long-range changes in the Mn_4CaO_5 environment can promote the stabilization of the S_2^{HS} state at the expense of the S_2^{LS} state as in the V185T mutant [69]. Similarly, a mutation of a Mn_4CaO_5 ligand that stabilizes the S_2^{HS} state, as the D170E mutation, also modifies the H-bond network, *e.g.* [87].

The S-state dependent proton release shows a correlation between the formation of the S_2^{HS} state and the release of a proton in the S_1 to S_2 transition. This correlation does not necessarily imply a causality even if that seems reasonable. Under conditions where the S_2^{LS} state is the stable S_2 state, this proton release occurs in the $S_2^{LS}Tyr_Z^\bullet$ state since it is well established that it precedes the electron transfer step [56-60]. In the model proposed here, this proton release would result in the formation of the $S_2^{HS}Tyr_Z^\bullet$ state which would be the competent configuration for the formation of S_3. Under conditions where the S_2^{HS} state becomes the stable S_2 state, the release of the proton is proposed to occur in the S_1 to S_2

transition. At this step, we cannot discard the possibility that the S_2^{LS} state is a transient state is a sequence of events as $S_1Tyr_Z^\bullet \rightarrow S_2^{LS}Tyr_Z \rightarrow S_2^{HS}Tyr_Z$. Because the exchange of Ca^{2+} with Sr^{2+} stabilizes the S_2^{HS} state, in the context of the model proposed in [39,40], that would mean that in PSII/Sr the pK of O4 increases and/or that of W1, considered to be the deprotonation site *via* a channel that includes Asp61 [42,88-90], decreases since the apparent pK of the $g \sim 2.0$ to $g \sim 4.8$ conversion is lower in PSII/Sr than in PSII/Ca [36].

In line with this, we have observed that in a small proportion of PSII/Sr, the S_2-state produced by an illumination at 180 K gave rise to a $g \sim 4.3$ signal (equivalent to the $g \sim 4.1$ signal in PSII/Ca) that is converted into a $g \sim 4.8$-4.9 signal upon a short warming at ~ 200 K in the dark [91]. This conversion correlates well with the proton movement proposed in [39,40] that would be blocked at 180 K and allowed at 200 K. Pushing further the interpretation in the context of the Corry and O'Malley model, the $g \sim 4.1$-4.3 signal would correspond to the $S = 5/2$ S_2-state with O4 protonated and the $g \sim 4.8$-4.9 signal would correspond to the $S = 7/2$ S_2-state with O4 deprotonated. In addition, preliminary experiments done in plant PSII under conditions in which the S_2^{HS} form exhibits the $g \sim 4.1$-4.3 signal suggest that this S_2^{HS} state is unable to progress to the S_3 state at 198 K and that, even at pH $\sim$ 8 (unpublished). In PSII/Ca, upon a Cl^-/I^- exchange, an illumination at 198 K results in the formation of a S_2^{HS} state with a signal at $g \sim 4.09$ that is unable to progress to S_3 at low temperatures [91]. Since this chloride is proposed to be involved in the function of the "O4" proton channel [90], the inhibition of the $g \sim 4.09$ state (likely a $S = 5/2$ state) to the $g \sim 4.8$-4.9 state (the $S = 7/2$ state) in PSII/Ca with I^- could be due an altered function of the "O4" proton channel making the deprotonation of W1 difficult and thus in the inhibition of the formation of the $S = 7/2$ state in the context of the Corry and O'Malley model [39,40].

Interestingly, a $g \sim 4.8$ EPR signal with a resolved hyperfine structure was recently detected in plant PSII after the removal of the extrinsic proteins [92] and it would be interesting to know if this state is able to progress to S_3 at low temperatures.

In a recent computational work, the consequences of the Ca^{2+}/Sr^{2+} exchange on the S_2 to S_3 transitions has been analyzed [93]. In this model, two transient states with a closed cubane S_2^{HS} exhibiting a $g = 4.1$ configuration have been probed. It was found that the more stable S_2^{HS} state, in PSII/Ca, was with $W3 = OH^-$ (with pK = 6.5) and with a neutral His190 whereas in PSII/Sr the more stable state was with $W3 = OH_2$ (with pK = 10.3) and with His190(H^+). If we do not consider the validity or not of the closed cubane option, something that is not a minor issue, these findings, which take into account principally the pK of W3,

seems to us difficult to reconcile with our experimental data since in PSII/Ca we would expect W3 as largely deprotonated at pH 8.0 with a pK value of 7 whereas the S_2 state is mostly in the low-spin configuration [36].

A proton leaving W1 is, in several models, proposed to be transferred to either the Asp61, *e.g.* [40,76,80], or to a close by water molecule (W19 in [40]) thus replacing the H^+ of W19 which has moved onto O4. In other mechanisms [21,77] a proton moving towards either Asp61 or W25 would originate from W3, before W3 leaves the Ca^{2+} and binds to Mn1. In all cases, the proton that is released into the bulk cannot be the proton moving onto either Asp61 or W19 or W25, but a proton connected to these proton acceptors *via* a H-bond network reorganized differently at pH 7.0 in PSII/Sr and PSII/Ca. That would explain why the proton released in the S_1 to S_2^{HS} transition in PSII/Sr at pH 7.0 seems not missing in the S_2^{HS} to S_3 transition.

The issue concerning the proton and water movements in the S_2 to S_3 transition has been addressed recently by following the structural changes in the water and proton channels at times 50 µs, 150 µs, 250 µs, after the second flash [22]. The pieces of information obtained are impressive and impossible to be listed here. One of the conclusions is that the "O1" channel is more likely a water channel than a proton channel. This in agreement with the analysis of the Arg323Glu mutant in which the dielectric relaxation of the protein in the Tyr_Z to P_{680}^+ electron transfer is delayed whereas no change in the proton release are observed [67]. It remains that the state, identified in [22], 50 µs after the second flash in the S_2 to S_3 transition could correspond to the structural arrangement favoring the formation of the S_2^{HS} state. Indeed, 50 µs after the second flash, the proton release has already occurred almost completely. Secondly, the structural changes observed at longer times than 50 µs are those accompanying the electron transfer between the Mn_4CaO_5 complex and $Tyr_Z^\bullet$.

Table 2 shows the $t_{1/2}$ of the kinetics for the proton releases and for the 440 nm-*minus*-424 nm differences from the curves in Figures 4 and 5. The $t_{1/2}$ values are the time at half of the decay of the kinetics determined without a fitting. It should be kept in mind that the kinetics of the 440 nm-*minus*-424 nm differences concerning the proton release steps are necessarily faster than the kinetics of the appearance of the proton into the bulk which is the last step of the proton egress mechanism, see [60,62].

Table 2 shows that the proton uptake associated with the reduction of the non heme iron after the 1st flash is affected in PSII/Sr at pH 6.0, *i.e.* at a pH value where there is no contamination of the kinetics by a proton release in contrast to the situation at pH 7.0. In PSII/Ca, a pH dependence between 6.0 and 7.0 is not observed. Unfortunately, there is no

report in the literature about the electron transfer from Q_A^- to the oxidized non-heme iron in PSII/Sr that could help us to understand the origin of this pH dependence. It was reported that the Ca^{2+}/Sr^{2+} exchange slightly up-shifted the $E_m(Q_A/Q_A^-)$ by $\sim +27$ mV [94], see however [95]. This increase could slightly slow down the reduction of oxidized non-heme iron at pH 6.0 when compared to PSII/Ca. However, the pH effect observed here on the rate of the proton uptake in PSII/Sr cannot be related to the pK values of the D1-H215 and Glu/Asp residues responsible for the E_m of the non-heme iron [96]. The positive point remains that at pH 7.0, the kinetics of the proton uptake are similar in PSII/Ca and PSII/Sr, which allows an easier comparison of the kinetics of the proton releases.

After the 3rd flash, the release of the first proton in the S_3 to S_0 transition, *i.e.* in the $S_3Tyr_Z^\bullet \rightarrow (S_3Tyr_Z^\bullet)'$ step, occurs at a similar rate in the four samples with a $t_{1/2}$ of 40 µs. This $t_{1/2}$ is in agreement with the fastest phase in the 440 nm-*minus*-424 nm difference. The kinetics of the 2nd proton in PSII/Sr at pH 7.0, *i.e.* in the $(S_3Tyr_Z^\bullet)' \rightarrow S_0Tyr_Z$ step, with $t_{1/2} \leq$ 5 ms, seems faster than expected from the known slowing down from 1-2 ms in PSII/Ca to 5 ms in PSII/Sr for this step [66] whereas this slowing down is observed in the kinetics of the 440 nm-*minus*-424 nm difference at both pH 6.0 and pH 7.0. There is no clear explanation now for that and this observation deserves to be further studied in the future because it is a potential source of information on the mechanism of water oxidation. At least, it is not due to a drift of the pH value. Indeed, *i*) above pH 7.0 the sample is rapidly damaged something that is not supported by the kinetics after the 1st, 2nd and 4th flashes and *ii*) below pH 7.0 the kinetics of the proton release would be similar to that of the electron transfer something not observed.

In the the $S_0Tyr_Z^\bullet$ to S_1Tyr_Z transition, *i.e.* after the 4th flash, the proton release occurred with a similar rate in the four samples with a $t_{1/2}$ of 200-300 µs. In this S-state transition, the proton release in PSII/Ca at pH 6.0 and pH 7.0 and in PSII/Sr at pH 7.0 occurs after the electron transfer that has a $t_{1/2}$ of 10-20 µs as previously discussed in detail *versus* the literature [60]. In PSII/Sr at pH 6.0 the kinetics of the 440 nm-*minus*-424 nm difference seems to have a single phase with a $t_{1/2}$ of 500 µs whereas the proton is released with a $t_{1/2}$ of 300 µs. This could suggest that at pH 6.0, in PSII/Sr, the proton release either precedes or occurs at the same time as the electron transfer at the opposite of the situation in PSII/Ca and PSII/Sr at pH 7.0.

Conclusions

Both the stoichiometry and the kinetics of the proton release were followed in PSII/Ca and PSII/Sr at pH 6.0 and pH 7.0. At pH 7.0, the PSII/Sr exhibits a S_2^{HS} configuration in half of the centers whereas in PSII/Ca at pH 7.0 as at pH 6.0 and in PSII/Sr at pH 6.0 the PSII is in a S_2^{LS} configuration after 1 flash. Several differences between PSII/Ca and PSII/Sr not yet reported in the literature or better seen here, were found. Among them, the 440 nm-*minus*-424 nm kinetics clearly show that the Ca^{2+}/Sr^{2+} exchange is slowing down by a factor 10 the $S_1Tyr_Z^{\bullet} \rightarrow S_2$ transition. Previous measurements at 291 nm [66] were less accurate because at this wavelength the absorption coefficient of $S_1Tyr_Z^{\bullet}$ and S_2 are close. In addition, in the S_0 to S_1 transition, the electron transfer seems slowed down in PSII/Sr at pH 6.0 to occur almost coupled to the electron transfer in contrast to PSII/Ca at pH 6.0 in which the proton is released after the electron transfer.

The fittings of the oscillations with a period of four strongly indicate that, when half of the centers are in S_2^{HS} after one flash illumination, about 0.5 proton is released in the S_1 to S_2 transition. It is therefore suggested that the proton that is released into the bulk in the S_2 to S_3 transition, when the S_2^{LS} state is the most stable configuration, is released in the $S_2^{LS}Tyr_Z^{\bullet} \rightarrow S_2^{HS}Tyr_Z^{\bullet}$ transition before the electron transfer from the cluster to $Tyr_Z^{\bullet}$ occurs. Such a model would imply that this proton would be missing in the following S_2^{HS} to S_3 transition. Instead, it is principally missing either in the S_3 to S_0 transition or in the S_0 to S_1 transition while the global charge probed by the electrochromism of P_{D1} increases in the S_2^{HS} to S_3 transition in PSII/Sr at pH 7.0 thus suggesting that less proton(s) are released. Further studies are required for a better understanding of the mechanism that links the proton movements in and around the cluster and the proton movements in the channels ultimately resulting by the release of protons into the bulk.

Acknowledgments

Rappaport who passed away too much early, Catherine Berthomieu, Rainer Hienerwadel, Julien Sellés and many other colleagues whose list would be too long here but who, I hope, will recognize themselves.

Table 1: Fitted values for the data shown in Figures 1 and 3.

sample	offset	dye					440 nm-*minus*-424 nm			
		h_0 $S_0 \rightarrow S_1$	h_1 $S_1 \rightarrow S_2$	h_2 $S_2 \rightarrow S_3$	h_3 $S_3 \rightarrow S_0$	Σh_i	ε_0 $S_0 \rightarrow S_1$	ε_1 $S_1 \rightarrow S_2$	ε_2 $S_2 \rightarrow S_3$	$-\Sigma \varepsilon_i$ $S_3 \rightarrow S_0$
PSII/Ca pH 6.0	1000	-1879 (1.2)	0 (0)	-1764 (1.13)	-2627 (1.68)	-6270	-149	1306	-90	-1067
PSII/Ca pH 7.0	-800	716 (0.77)	19 (0.02)	1057 (1.13)	1946 (2.08)	3738	-257	1792	-131	-1404
PSII/Sr pH 6.0	600	-1790 (1.35)	0 (0)	-1476 (1.11)	-2054 (1.54)	-5320	-192	944	-161	-591
PSII/Sr pH 7.0	-800	873 (1.02)	405 (0.47)	884 (1.03)	1266 (1.48)	3428	-63	1080	219	-1237
Plant PSII, pH 6.0[1]		(1.52)	(0.05)	(1.0)	(1.43)					
Plant PSII pH 7.0[1]		(1.10)	(0.32)	(1.0)	(1.58)					

$\Delta I/I \times 10^6$ values corresponding to the best fittings shown in Figures 1 and 3. The h_0, h_1, h_2 and h_3 values are the $\Delta I/I$ changes associated to the changes in the protonation state of the dyes in the S_0 to S_1, S_1 to S_2, S_2 to S_3 and S_3 to S_0 transitions, respectively. The Σh_i value corresponds to the total absorption change for one turnover (*i.e.* $h_0 + h_1 + h_2 + h_3$) which corresponds to 4 H^+. The values in brackets are the ratio $h_i/\Sigma h_i$ which corresponds to stoichiometry of the proton released in the corresponding transition. The ε_0, ε_1, ε_2 values are the extinction coefficients corresponding to the S_0 to S_1, S_1 to S_2 and S_2 to S_3 transitions, respectively. By definition [63], the extinction coefficient of the S_3 to S_0 transition is $-\Sigma \varepsilon_I$ (*i.e.* $-(\varepsilon_0 + \varepsilon_1 + \varepsilon_2)$). In all the fittings the miss parameter, considered as identical in all the transitions, was found to be between 8 and 10 % and the proportion of centers in S_1 between 90 and 100 %. [1]Data taken in [62].

Table 2 : Approximate $t_{1/2}$ values of the kinetics shown in Figures 4 and 5.

Sample	dye				440 nm-*minus*-424 nm			
	4th flash $S_0 \rightarrow S_1$	1st flash $S_1 \rightarrow S_2$	2nd flash $S_2 \rightarrow S_3$	3rd flash $S_3 \rightarrow S_0$	4th flash $S_0 \rightarrow S_1$	1st flash $S_1 \rightarrow S_2$	2nd flash $S_2 \rightarrow S_3$	3rd flash $S_3 \rightarrow S_0$
PSII/Ca pH 6.0	(-) 200 µs	(+) 300 µs	(-) 60 µs	(-) 40 µs, 1-2 ms	10-20 µs, 200 µs	20-30 µs	10-20 µs, 200 µs	20 µs, 1 ms
PSII/Ca pH 7.0	(-) 200 µs	(+) <200 µs	(-) 60 µs	(-) 40 µs, 2 ms	10-20 µs, 200 µs	20-30 µs	20 µs, 200 µs	20 µs, 1 ms
PSII/Sr pH 6.0	(-) 300 µs	(+) 1 ms	(-) 60 µs	(-) 40 µs, 5 ms	500 µs	200 µs	20 µs, 200 µs	10 µs, 5 ms
PSII/Sr pH 7.0	(-) 200 µs	(+) 200 µs	(-) 60 µs	(-) 40 µs, ≤5 ms	10-20 µs, 300 µs	200 µs (20 µs?)	20 µs, 200 µs	10-20 µs, 5 ms

Approximate $t_{1/2}$ values of the kinetics in Figures 4 and 5 after 4th, 1st, 2nd and 3rd flashes, *i.e.* in the S_0 to S_1, S_1 to S_2, S_2 to S_3 and S_3 to S_0 transitions, respectively, in PSII/Ca and PSII/Sr at pH 6.0 and PH 7.0. The sign in brackets indicates a proton uptake with (+) and a proton release with (-).

Legend of figures

Figure 1:

Sequence of the amplitude of the absorption changes using a series of saturating flashes (spaced 400 ms apart). The full circles, shows the absorbance changes at 575 nm of either bromocresol purple (150 µM) at pH 6.0 (Panels A and B, purple full circles) or at 547 nm of neutral red (40 µM) at pH 7.0 (Panels C and D, red full circles). The measurements were done with PSII/Ca in Panels A and C and with PSII/Sr in Panels B and D. The samples ([Chl] = 25 µg mL^{-1}) were dark-adapted for 1 h at room temperature before the addition of 100 µM PPBQ dissolved in dimethyl sulfoxide and 100 µM ferricyanide. The $\Delta I/I$ were measured 100 ms after each flash. The black crosses joined by a continuous line are the fits of the data with the parameters listed in Table 1.

Figure 2:

Results of the fittings at pH 6.0 for PSII/Ca in Panel A and for PSII/Sr in Panel B and at pH 7.0 for PSII/Ca in Panel C and for PSII/Sr in Panel D. The X-axis corresponds to different values of the offset, in $\Delta I/I$ units, which were tested in the fitting procedure. This offset corresponds to the sum of the proton uptake and the amplitude of the drift 100 ms after the flash. The values h_0 (in green), h_1 (in black), h_2 (in red), h3 (in blue) are the fitted $\Delta I/I$ values corresponding to the release of proton(s) in the S_0 to S_1, S_1 to S_2, S_2 to S_3 and S_3 to S_0 transitions, respectively, for each value of the offset. The yellow curve corresponds to the sum of the squares of the residues calculated from the 2nd to the 40th flash. At pH 6.0, the sum of the squares of the residues was multiplied by -1 for a better visualisation of the curves in the graph.

Figure 3:

Sequence of the amplitude of the 440 nm-*minus*-424 nm differences using a series of saturating flashes (spaced 400 ms apart). The red full circles, shows the experimental data and the black crosses joined by a continuous line are the fits of the data with the parameters listed in Table 1. Panel A, PSII/Ca at pH 6.0; Panel B, PSII/Sr at pH 6.0; Panel C, PSII/Ca at pH 6.0; Panel D, PSII/Sr at pH 7.0. The samples ([Chl] = 25 µg mL^{-1}) were dark-adapted for 1 h at room temperature before the addition of 100 µM PPBQ dissolved in dimethyl sulfoxide. The $\Delta I/I$ were measured 100 ms after each flash.

Figure 4:

Time-courses of the absorption changes of bromocresol purple at either 575 nm (Panels A and B) or neutral red at 547 nm (Panels C and D) after the 1st flash (black points), the 2nd flash (red points), the 3rd flash (blue points), and the 4th flash (green points) given to either dark-adapted PSII/Ca (Panels A and C) or PSII/Sr (Panels B and D). The dashed lines are spline curves joining the experimental data points. Same other conditions as in Figure 1.

Figure 5:

Time-courses of the absorption change differences 440 nm-*minus*-424 nm after the 1st flash (black), the 2nd flash (red), the 3rd flash (blue), and the 4th flash (green) given to either dark-adapted PSII/Ca (Panels A and C) or PSII/Sr (Panels B and D) at either pH 6.0 (Panels A and C) or pH 7.0 (Panels B and D). The dashed lines are a spline curves joining the experimental data points. Same other conditions as in Figure 3.

References

1. T. Oliver, P. Sánchez-Baracaldo, A.W. Larkum, A.W. Rutherford, T. Cardona, Time-resolved comparative molecular evolution of oxygenic photosynthesis, Biochim. Biophys. Acta 1862 (2021) 148400. https://doi.org/10.1016/j.bbabio.2021.148400.

2. Y. Umena, K. Kawakami, J-R. Shen, N. Kamiya, Crystal structure of oxygen-evolving Photosystem II at a resolution of 1.9 angstrom, Nature 473 (2011) 55–60. https://doi.org/10.1038/nature09913

3. M. Suga, F. Akita, K. Hirata, G. Ueno, H. Murakami, Y. Nakajima, T. Shimizu, K. Yamashita, M. Yamamoto, H. Ago, J-R. Shen, Native structure of Photosystem II at 1.95 angstrom resolution viewed by femtosecond X-ray pulses, Nature (2015) 517: 99–103. https://doi.org/10.1038/nature13991

4. C.J. Gisriel, J. Wang, J. Liu, D.A. Flesher, K.M. Reiss, H-L. Huang, K.R. Yang, W.H. Armstrong, M.R. Gunner, V.S. Batista, R.J. Debus, G.W. Brudvig, High-resolution cryo-electron microscopy structure of Photosystem II from the mesophilic cyanobacterium, *Synechocystis* sp. PCC 6803, Proc. Natl. Acad. Sci. USA 119 (2022) e2116765118. https://doi.org/10.1073/pnas.2116765118

5. A.R. Holzwarth, M.G. Müller, M. Reus, M. Nowaczyk, J. Sander, M. Rögner, Kinetics and mechanism of electron transfer in intact Photosystem II and in the isolated reaction center: pheophytin is the primary electron acceptor, Proc. Natl. Acad. Sci. USA 103 (2006) 6895–6900. https://doi.org/10.1073/pnas.0505371103

6. E. Romero, V.I. Novoderezhkin, R. van Grondelle, Quantum design of photosynthesis for bio-inspired solar-energy conversion, Nature 543 (2017) 355–365. https://doi.org/10.1038/nature22012

7. W. Lubitz, M. Chrysina, N. Cox, Water oxidation in Photosystem II, Photosynth. Res. 142 (2019) 105–125. https://doi.org/10.1007/s11120-019-00648-3 .

8. C. Fufezan, C.-X. Zhang, A. Krieger-Liszkay, A.W. Rutherford, Secondary quinone in Photosystem II of *Thermosynechococcus elongatus*: Semiquinone-iron EPR signals and temperature dependence of electron transfer, Biochemistry 44 (2005) 12780–12789. https://doi.org/10.1021/bi051000k

9. A. Sedoud, N. Cox, M. Sugiura, W. Lubitz, A. Boussac, A.W. Rutherford, The semiquinone-iron complex of Photosystem II: EPR signals assigned to the low field edge of the ground state doublet of $Q_A^{\bullet-}Fe^{2+}$ and $Q_B^{\bullet-}Fe^{2+}$, Biochemistry 50 (2011) 6012–6021. https://doi.org/10.1021/bi200313p

10. A. Boussac, M. Sugiura, F. Rappaport, Probing the quinone binding site of Photosystem II from *Thermosynechococcus elongatus* containing either PsbA1 or PsbA3 as the D1 protein through the binding characteristics of herbicides, Biochim. Biophys. Acta 1807 (2010) 119–129. https://doi.org/10.1016/j.bbabio.2010.10.004

11. S. de Causmaecker, J.S. Douglass, A. Fantuzzi, W. Nitschke, A.W. Rutherford, Energetics of the exchangeable quinone, Q_B, in Photosystem II, Proc. Natl. Acad. Sci. USA 116 (2019) 19458–19463. www.pnas.org/cgi/doi/10.1073/pnas.1910675116

12. P, Joliot, G. Barbieri, R, Chabaud, A new model of photochemical centers in system 2, Photochem. Photobiol. 10 (1969) 309–329. https://doi.Org/10.1111/j.1751-1097.1969.tb05696.x

13. B. Kok, B. Forbush, M. McGloin, Cooperation of charges in photosynthetic O_2 evolution–I. A linear four step mechanism, Photochem. Photobiol. 11 (1970) 457–475. https://doi.org/10.1111/j.1751-1097.1970.tb06017.x

14. I.D. Young, M. Ibrahim, R. Chatterjee, S. Gul, F.D. Fuller, S. Koroidov, A.S. Brewster, R. Tran, R. Alonso-Mori, T. Kroll, T. Michels-Clark, H. Laksmono, R.G. Sierra, C.A. Stan, R. Hussein, M. Zhang, L. Douthit, M. Kubin, C. de Lichtenberg, L. Vo Pham, H. Nilsson, M. Hon Cheah, D. Shevela, C. Saracini, M.A. Bean, I. Seuffert, D. Sokaras, T-C. Weng, E. Pastor, C. Weninger, T. Fransson, L. Lassalle, P. Bräuer, P. Aller, P.T. Docker, B. Andi, A.M. Orville, J.M. Glownia, S. Nelson, M. Sikorski, D. Zhu, M.S. Hunter, T.J. Lane, A. Aquila, J. E. Koglin, J. Robinson, M. Liang, S. Boutet, A.Y. Lyubimov, M. Uervirojnangkoorn, N.W. Moriarty, D. Liebschner, P.V. Afonine, D.G. Waterman, G. Evans, P. Wernet, H. Dobbek, W.I. Weis, A.T. Brunger, P.H. Zwart, P.D. Adams, A. Zouni, J. Messinger, U. Bergmann, N.K. Sauter, J. Kern, V.K. Yachandra, J.unko Yano, Structure of photosystem II and substrate binding at room temperature, Nature 540 (2013) 453–474. https://doi.org/doi:10.1038/nature20161

15. J.M. Wang, C.J. Gisriel, K. Reiss, H.L. Huang, W.H. Armstrong, G.W. Brudvig, V.S. Batista, Heterogeneous composition of oxygen-evolving complexes in crystal structures of dark-adapted Photosystem II, Biochemistry 60 (2021) 3374–3384. https://doi.org/10.1021/acs.biochem.1c00611

16. M. Askerka, G.W. Brudvig, V.S. Batista, The O_2-evolving complex of Photosystem II: Recent insights from quantum mechanics/molecular mechanics (QM/MM), Extended X-ray absorption fine structure (EXAFS), and femtosecond X-ray crystallography data, Acc. Chem. Res. 50 (2017) 41–48. https://doi.org/10.1021/acs.accounts.6b00405

17. H. Chen, G.C. Dismukes, D.A. Case, Resolving ambiguous protonation and oxidation states in the oxygen evolving complex of Photosystem II, J. Phys. Chem. B 122 (2018), 8654–8664. https://doi.org/10.1021/acs.jpcb.8b05577

18. D.A. Pantazis, Evaluation of new low-valent computational models for the oxygen-evolving complex of photosystem II, Chem. Phys. Let. 753 (2020) 137629. https://doi.org/10.1016/j.cplett.2020.137629

19. M. Shoji, H. Isobe, S. Yamanaka, M. Suga, F. Akita, J-R. Shen, K.Yamaguchi, On the guiding principles for lucid understanding of the damage-free S_1 structure of the $CaMn_4O_5$ cluster in the oxygen evolving complex of photosystem II, Chem. Phys. Lett. 627 (2015) 44–52. https://doi.org/10.1016/j.cplett.2015.03.033

20. M. Drosou, G. Zahariou, D.A. Pantazis, Orientational Jahn–Teller isomerism in the dark-stable state of nature's water oxidase, Angew. Chem. Int. Ed. 60 (2021) 13493–13499. https://doi-org.insb.bib.cnrs.fr/10.1002/anie.202103425C

21. M. Ibrahim, T. Fransson, R. Chatterjee, M.H. Cheah, R. Hussein, L. Lassalle, K.D. Sutherlin, I.D. Young, F.D. Fuller, S. Gul, I.S. Kim, P.S. Simon, C. de Lichtenberg, P. Chernev, I. Bogacz, C.C. Pham, A.M. Orville, N. Saichek, T. Northen, A. Batyuk, S. Carbajo, R. Alonso-Mori, K. Tono, S. Owada, A. Bhowmick, R. Bolotovsky, D. Mendez, N.W. Moriarty, J.M. Holton, H. Dobbek, A.S. Brewster, P.D. Adams, N.K. Sauter, U. Bergmann, A. Zouni, J. Messinger, J. Kern, V.K. Yachandra, J. Yano, Untangling the sequence of events during the $S_2 \rightarrow S_3$ transition in Photosystem II and implications for the water oxidation mechanism, Proc. Nat. Acad. Sci. USA 117 (2020) 12624–12635. https://doi.org/10.1073/pnas.2000529117

22. R. Hussein, M. Ibrahim, A. Bhowmick, P.S. Simon, R. Chatterjee, L. Lassalle, M. Doyle, I. Bogacz, I-S. Kim, MH. Cheah, S. Gul, C. de Lichtenberg, P. Chernev, C.C. Pham, I.D. Young, S. Carbajo, F.D. Fuller, R. Alonso-Mori, A. Batyuk, K.S. Sutherlin, A.S. Brewster, R. Bolotovsky, D. Mendez, J.M. Holton, N.W. Moriarty, P.D. Adams, U. Bergmann, N.K. Sauter, H. Dobbek, J. Messinger, A. Zouni, J. Kern, V.K. Yachandra, J. Yano, Structural dynamics in the water and proton channels of Photosystem II during the S_2 to S_3 transition, Nat. Commun. 12 (2021) 6531. https://doi.org/10.1038/s41467-021-26781-z

23. H.J. Li, Y. Nakajima, T. Nomura, M. Sugahara, S. Yonekura, S.K. Chan, T. Nakane, T. Yamane, Y. Umena, M. Suzuki, T. Masuda, T. Motomura, H. Naitow, Y. Matsuura, T. Kimura, K. Tono, S. Owada, Y. Joti, R. Tanaka, E. Nango, F. Akita, M. Kubo, S. Iwata, J-R. Shen, M. Suga, Capturing structural changes of the S_1 to S_2 transition of Photosystem II using

time-resolved serial femtosecond crystallography, IUCRJ 8 (2021) 431–443. https://doi.org/10.1107/S2052252521002177

24. M. Suga, F. Akita, K. Yamashita, Y. Nakajima, G. Ueno, H.J. Li, T. Yamane, K. Hirata, Y. Umena, S. Yonekura, L.J. Yu, H. Murakami, T. Nomura, T. Kimura, M. Kubo, S. Baba, T. Kumasaka, K. Tono, M. Yabashi, H. Isobe, K. Yamaguchi, M. Yamamoto, H. Ago, J-R. Shen, An oxyl/oxo mechanism for oxygen-oxygen coupling in PSII revealed by an x-ray free-electron laser, Science 366 (2019) 334–338. https://doi.org/10.1126/science.aax6998

25. L. Rapatskiy, N. Cox, A. Savitsky, W.M. Ames, J. Sander, M.M. Nowaczyk, M. Rögner, A. Boussac, F. Neese, J. Messinger, W. Lubitz, Detection of the water-binding sites of the oxygen-evolving complex of Photosystem II using W-Band ^{17}O Electron-Electron Double Resonance-Detected NMR spectroscopy, J. Am. Chem. Soc. 134 (2012) 16619–16634. https://doi.org/10.1021/ja3053267

26. S.L. Dexheimer, M.P. Klein, Detection of a paramagnetic intermediate in the S_1 state of the photosynthetic oxygen-evolving complex, J. Am. Chem. Soc. 114 (1992) 2821–2826. https://doi.org/10.1021/ja00034a010

27. T. Yamauchi, H. Mino, T. Matsukawa, A. Kawamori, T.-A. Ono, Parallel polarization electron paramagnetic resonance studies of the S_1-State manganese cluster in the photosynthetic oxygen-evolving system, Biochemistry 36 (1997) 7520–7526. https://doi.org/10.1021/bi962791g

28. K.A. Campbell, J.M. Peloquin, D.P. Pham, R.J. Debus, R.D. Britt, Parallel polarization EPR detection of an S_1-State "Multiline" EPR signal in Photosystem II particles from *Synechocystis* sp. PCC 6803, J. Am Chem. Soc. 120 (1998) 447–448. https://doi.org/10.1021/ja972693y

29. G.C. Dismukes, Y. Siderer, Intermediates of a polynuclear manganese center involved in photosynthetic oxidation of water, Proc. Natl. Acad. Sci. U. S. A. 78 (1981), 274–278. https://doi.org/10.1073/pnas.78.1.274

30. J.M. Peloquin, K.A. Campbell, D.W. Randall, M.A. Evanchik, V.L. Pecoraro, W.H. Armstrong, R.D. Britt, Mn-55 ENDOR of the S_2-state multiline EPR signal of Photosystem II: Implications on the structure of the tetranuclear Mn cluster, J. Am. Chem. Soc. 122 (2000) 10926–10942. https://doi.org/10.1021/ja002104f

31. N. Cox, L. Rapatskiy, J-H. Su, D.A. Pantazis, M. Sugiura, L. Kulik, P. Dorlet, A.W. Rutherford, F. Neese, A. Boussac, W. Lubitz, J. Messinger, Effect of Ca^{2+}/Sr^{2+} substitution on the electronic structure of the oxygen-evolving complex of Photosystem II: A combined

multifrequency EPR, Mn-55-ENDOR, and DFT study of the S_2 state, J. Am Chem. Soc. 133 (2011) 3635–3648. https://doi.org/10.1021/ja110145v

32. J.-L. Zimmermann, A.W. Rutherford, Electron paramagnetic resonance studies of the oxygen-evolving enzyme of Photosystem II, Biochim. Biophys. Acta 767 (1984), 160–167. https://doi.org/10.1016/0005-2728(84)90091-4

33. J.L. Casey, K. Sauer, Electron paramagnetic resonance detection of a cryogenically photogenerated intermediate in photosynthetic oxygen evolution, Biochim. Biophys. Acta 767 (1984), 21–28. https://doi.org/10.1016/0005-2728(84)90075-6

34. A. Boussac, S. Un, O. Horner, A.W. Rutherford, High spin states ($S \geq 5/2$) of the photosystem II manganese complex, Biochemistry 37 (1998), 4001–4007. https://doi.org/10.1021/bi9728710

35. A. Boussac, H. Kuhl, S. Un, M. Rögner, A.W. Rutherford, Effect of near-infrared light on the S_2-state of the manganese complex of photosystem II from *Synechococcus elongatus*, Biochemistry 37 (1998), 8995–9000. https://doi.org/10.1021/bi980195b

36. A. Boussac, I. Ugur, A. Marion, M. Sugiura, V.R.I. Kaila, A.W. Rutherford, The low spin - high spin equilibrium in the S_2-state of the water oxidizing enzyme, Biochim. Biophys. Acta 1859 (2018), 342–356. https://doi.org/10.1016/j.bbabio.2018.02.010

37. A. Boussac, Temperature dependence of the high-spin S_2 to S_3 transition in Photosystem II: Mechanistic consequences, Biochim. Biophys. Acta 1860 (2019) 508–518. https://doi.org/10.1016/j.bbabio.2019.05.001

38. D.A. Pantazis, W. Ames, N. Cox, W. Lubitz, F. Neese, Two interconvertible structures that explain the spectroscopic properties of the oxygen-evolving complex of Photosystem II in the S_2 state, Angew. Chem. Intl. Ed. 51 (2012), 9935–9940. https://doi.org/10.1002/anie.201204705

39. T.A. Corry, P.J. O'Malley, Proton isomers rationalize the high- and low-spin forms of the S_2 state intermediate in the water-oxidizing reaction of Photosystem II, J. Phys. Chem. Lett. 10 (2019) 5226–5230. https://doi.org/10.1021/acs.jpclett.9b01372

40. T.A. Corry, P.J. O'Malley, Molecular identification of a high-spin deprotonated intermediate during the S_2 to S_3 transition of nature's water-oxidizing complex, J. Am. Chem. Soc. 142 (2020) 10240-10243. https://doi.org/10.1021/jacs.0c01351

41. D.A. Pantazis, Missing pieces in the puzzle of biological water oxidation, ACS Catal. 8 (2018) 9477–9507. https://doi.org/10.1021/acscatal.8b01928

42. D. Narzi, D. Bovi, L. Guidoni, Pathway for Mn-cluster oxidation by tyrosine-Z in the S_2 state of photosystem II, Proc. Nat. Aca. Sci. USA 111 (2014) 8723–8728. https://doi.org/10.1073/pnas.1401719111

43. P.E.M. Siegbahn, The S_2 to S_3 transition for water oxidation in PSII (Photosystem II), revisited, Phys. Chem. Chem. Phys. 20 (2018) 22926–22931. https://doi.org/10.1039/C8CP03720E

44. Y. Sanakis, J. Sarrou, G. Zahariou, V. Petrouleas, Q-band electron paramagnetic resonance studies of the S_3 state of the OEC of Photosystem II In: Allen J.F., Gantt E., Golbeck J.H., Osmond B. (eds), 2008, Photosynthesis. Energy from the Sun. Springer, Dordrecht. https://doi.org/10.1007/978-1-4020-6709-9_108

45. A. Boussac, M. Sugiura, A.W. Rutherford, P. Dorlet, Complete EPR spectrum of the S_3-state of the oxygen-evolving photosystem II, J. Am. Chem. Soc. 131 (2009) 5050–5051. https://doi.org/10.1021/ja900680t

46. N. Cox, M. Retegan, F. Neese, D.A. Pantazis, A. Boussac, W. Lubitz, Electronic structure of the oxygen evolving complex in photosystem II prior to O-O bond formation, Science 345 (2014) 804–808. https://doi.org/10.1126/science.1254910

47. D.A. Marchiori, R.J. Debus, R.D. Britt, Pulse EPR spectroscopic characterization of the S_3 state of the oxygen-evolving complex of Photosystem II isolated from *Synechocystis*, Biochemistry 59 (2020) 4864–4872. https://doi.org/10.1021/acs.biochem.0c00880

48. G. Zahariou, N. Ioannidis, Y. Sanakis, D.A. Pantazis, Arrested substrate binding resolves catalytic intermediates in higher-plant water oxidation, Angew. Chem. Intl. Ed. 60 (2020) 3156–3162. https://doi.org/10.1002/anie.202012304

49. M. Chrysina, E. Heyno, Y. Kutina, M. Reus, H. Nilsson, M.M. Nowaczyk, S. DeBeer, F. Neese, J. Messinger, W. Lubitz, N. Cox, Five-coordinate Mn^{IV} intermediate in the activation of nature's water splitting cofactor, Proc. Nat. Aca. Sci. USA 116 (2019) 16841–16846. https://doi.org/10.1073/pnas.1817526116

50. K.G.V. Havelius, J-H. Su, Y. Feyziyev, F. Mamedov, S. Styring, Spectral resolution of the split EPR signals induced by illumination at 5 K from the S_1, S_3, and S_0 states in Photosystem II, Biochemistry 45 (2006) 9279–9290. https://doi.org/10.1021/bi060698e

51. A. Boussac, M. Sugiura, T-L. Lai, A.W. Rutherford, Low-temperature photochemistry in Photosystem II from *Thermosynechococcus elongatus* induced by visible and near-infrared light, Phil. Trans. R. Soc. London Ser. B 363 (2008) 1203–1210. https://doi.org/10.1098/rstb.2007.2216

52. V. Krewald, F. Neese, D.A. Pantazis, Implications of structural heterogeneity for the electronic structure of the final oxygen-evolving intermediate in Photosystem II, J. Inorg. Biochem. 199 (2019) 110797. https://doi.org/10.1016/j.jinorgbio.2019.110797

53. M. Drosou, D.A. Pantazis, Redox isomerism in the S_3 state of the oxygen-evolving complex resolved by coupled cluster theory, Chem. Eur. J. 27 (2021) 12815–12825. https://doi.org/10.1002/chem.202101567

54. H. Isobe, M. Shoji, T. Suzuki, J-R. Shen, Spin, valence, and structural isomerism in the S_3 state of the oxygen-evolving complex of Photosystem II as a manifestation of multimetallic cooperativity, J. Chem. Theory Comput. 15 (2019) 2375–2391. https://doi.org/10.1021/acs.jctc.8b01055

55. H. Isobe, M. Shoji, T. Suzuki, J-R. Shen, K. Yamaguchi, Exploring reaction pathways for the structural rearrangements of the Mn cluster induced by water binding in the S_3 state of the oxygen evolving complex of Photosystem II, J. Photochem. Photobiol. A: Chemistry 405 (2021) 112905. https://doi.org/10.1016/j.jphotochem.2020.112905

56. A. Klauss, M. Haumann, H. Dau, Seven steps of alternating electron and proton transfer in Photosystem II water oxidation traced by time-resolved photothermal beam deflection at improved sensitivity, J. Phys. Chem. B 119 (2015) 2677–2689. https://doi.org/10.1021/jp509069p

57. I. Zaharieva, H. Dau, M. Haumann, Sequential and coupled proton and electron transfer events in the $S_2 \rightarrow S_3$ transition of photosynthetic water oxidation revealed by time-resolved X-ray absorption spectroscopy, Biochemistry 55 (2016) 6996–7004. https://doi.org/10.1021/acs.biochem.6b01078

58. Y. Okamoto, Y. Shimada, R. Nagao, T. Noguchi, Proton and water transfer pathways in the $S_2 \rightarrow S_3$ transition of the water-oxidizing complex in Photosystem II: Time-resolved infrared analysis of the effects of D1-N298A mutation and NO_3-substitution, J. Phys. Chem. B 125 (2021) 6864–6873. https://doi.org/10.1021/acs.jpcb.1c03386

59. S.M. Mausle, A. Abzaliyeva, P. Greife, P.S. Simon, R. Perez, Y. Zilliges, H. Dau, Activation energies for two steps in the $S_2 \rightarrow S_3$ transition of photosynthetic water oxidation from time-resolved single-frequency infrared spectroscopy, J. Chem. Phys. 153 (2020) 215101. https://doi.org/10.1063/5.0027995

60. A. Boussac, J. Sellés, M. Sugiura, What can we still learn from the electrochromic band-shifts in Photosystem II? Biochim. Biophys. Acta 1861 (2020) 148176. https://doi.org/10.1016/j.bbabio.2020.148176

61. V. Förster, W. Junge, Stoichiometry and kinetics of proton release upon photosynthetic water oxidation, Photochem. Photobiol. 41 (1985) 183–190. https://doi.org/10.1111/j.1751-1097.1985.tb03469.x

62. F. Rappaport, J. Lavergne, Proton release during successive oxidation steps of the photosynthetic water oxidation process - stoichiometries and pH-dependence, Biochemistry 30 (1991) 10004–10012. https://doi.org/10.1021/bi00105a027

63. J. Lavergne, Improved UV-visible spectra of the S-transitions in the photosynthetic oxygen-evolving system, Biochim. Biophys. Acta, 1060 (1991) 175–188. https://doi.org/10.1016/S0005-2728(09)91005-2

64. M. Sugiura, A. Boussac, T. Noguchi, F. Rappaport, Influence of Histidine-198 of the D1 subunit on the properties of the primary electron donor, P680, of Photosystem II in *Thermosynechococcus elongatus*, Biochim Biophys Acta 1777 (2008) 331–342. https://doi.org/10.1016/j.bbabio.2008.01.007

65. M. Sugiura, Y. Inoue, Highly purified thermo-stable oxygen evolving Photosystem II core complex from the thermophilic cyanobacterium *Synechococcus elongatus* having His-tagged CP43. Plant Cell Physiol 40 (1999)1219–1231. https://doi.org/10.1093/oxfordjournals.pcp.a029510

66. N. Ishida, M. Sugiura, F. Rappaport, T-L. Lai, A.W. Rutherford, A. Boussac, Biosynthetic exchange of bromide for chloride and strontium for calcium in the Photosystem II oxygen-evolving enzymes, J. Biol. Chem. 283 (2008) 13330–13340. https://doi.Org/10.1074/jbc.M710583200

67. M. Sugiura, T. Taniguchi, N. Tango, M. Nakamura, J. Sellés, A. Boussac, Probing the role of arginine 323 of the D1 protein in Photosystem II function, Physiol. Plant. 171 (2021) 183–199. https://doi.org/10.1111/ppl.13115

68. D. Béal, F. Rappaport, P. Joliot, A new high-sensitivity 10-ns time-resolution spectrophotometric technique adapted to in vivo analysis of the photosynthetic apparatus, Rev. Sci. Instrum. 70 (1999) 202–207. https://doi.org/10.1063/1.1149566

69. M. Sugiura, T. Tibiletti, I. Takachi, Y. Hara, S. Kanawaku, J. Sellés, A. Boussac, Probing the role of Valine 185 of the D1 protein in the Photosystem II oxygen evolution, Biochim. Biophys. Acta 1859 (2018) 1259–1273. https://doi.org/10.1016/j.bbabio.2018.10.003

70. F. Müh, A. Zouni, Extinction coefficients and critical solubilisation concentrations of Photosystems I and II from *Thermosynechococcus elongatus*, Biochim. Biophys. Acta 1708 (2005) 219–228. https://doi.org/10.1016/j.bbabio.2005.03.005

71. H. Nilsson, F. Rappaport, A. Boussac, J. Messinger, Substrate-water exchange in Photosystem II is arrested before dioxygen formation, Nat. Commun. 5 (2014) 4305. https://doi.org/10.1038/ncomms5305

72. F. Rappaport, M. Blanchard-Desce, J. Lavergne, Kinetics of electron-transfer and electrochromic change during the redox transitions of the photosynthetic oxygen-evolving complex, Biochim. Biophys. Acta 1184 (1994) 178–192. https://doi.org/10.1016/0005-2728(94)90222-4

73. C. Berthomieu, R. Hienerwadel, Iron coordination in Photosystem II: Interaction between bicarbonate and the Q(B) pocket studied by Fourier transform infrared spectroscopy, Biochemistry 40 (2001) 4044–4052. https://doi.org/10.1021/bi002236l

74. M. Kimura, Y. Kato, T. Noguchi, Protonation state of a key histidine ligand in the iron-quinone complex of Photosystem II as revealed by light-induced ATR-FTIR spectroscopy, Biochemistry 59 (2020) 4336–4343. https://doi.org/10.1021/acs.biochem.0c00810

75. M. Haumann, W. Junge, Extent and rate of proton release by photosynthetic water oxidation in thylakoids: electrostatic relaxation versus chemical production, Biochemistry 33 (1994) 864–872. https://doi.org/10.1021/bi00170a003

76. M. Retegan, N. Cox, W. Lubitz, F. Neese, D.A. Pantazis, The first tyrosyl radical intermediate formed in the S_2-S_3 transition of Photosystem II, Phys. Chem. Chem. Phys. 16 (2014) 11901–11910. https://doi.org/10.1039/C4CP00696H

77. I. Ugur, A.W. Rutherford, V.R.I. Kaila, Redox-coupled substrate water reorganization in the active site of Photosystem II - The role of calcium in substrate water delivery, Biochim. Biophys. Acta 1857 (2016) 740–748. https://doi.org/10.1016/j.bbabio.2016.01.015

78. J. Wang, M. Askerka, G.W. Brudvig, V.S. Batista, Crystallographic data support the carousel mechanism of water supply to the oxygen evolving complex of Photosystem II, ACS Energy Lett. 2 (2017) 2299–2306. https://doi.org/10.1021/acsenergylett.7b00750

79. D. Kaur, W. Szejgis, JJ. Mao, M. Amin, K.M. Reiss, M. Askerka, X.H. Cai, U. Khaniya, Y.Y Zhang, G.W. Brudvig, V.S. Batista, M.R. Gunner, Relative stability of the S_2 isomers of the oxygen evolving complex of Photosystem II, Photosynth. Res. 14 (2019) 331–341. https://doi.org/10.1007/s11120-019-00637-6

80. P.E.M. Siegbahn, Water oxidation mechanism in Photosystem II, including oxidations, proton release pathways, O—O bond formation and O_2 release, Biochim. Biophys. Acta 1827 (2013) 1003–1019. http://dx.doi.org/10.1016/j.bbabio.2012.10.006

81. K.R. Yang, K.V. Lakshmi, G.W. Brudvig, V.S. Batista, Is deprotonation of the oxygen-evolving complex of Photosystem II during the $S_1 \rightarrow S_2$ transition suppressed by proton

quantum delocalization?, J. Am. Chem. Soc. 143 (2021) 8324–8332. https://doi.org/10.1021/jacs.1c00633

82. D.A. Pantazis, The S_3 state of the oxygen-evolving complex: Overview of spectroscopy and XFEL crystallography with a critical evaluation of early-onset models for O–O bond formation, Inorganics 7 (2019) 55. https://doi.org/10.3390/inorganics7040055

83. H. Suzuki, M. Sugiura, T. Noguchi, Monitoring proton release during photosynthetic water oxidation in Photosystem II by means of isotope-edited infrared spectroscopy, J. Am. Chem. Soc. 131 (2009) 7849–7857. https://doi.org/10.1021/ja901696m

84. G. Bernát, F. Morvaridi, Y. Feyziyev, S. Styring, pH dependence of the four individual transitions in the catalytic S-cycle during photosynthetic oxygen evolution, Biochemistry 41 (2002) 5830–5843. https://doi.org/10.1021/bi011691u

85. F. Guerra, M. Siemers, C. Mielack, A-N. Bondar, Dynamics of long-distance hydrogen-bond networks in Photosystem II, J. Phys. Chem. B 122 (2018) 4625–4641. https://doi.org/10.1021/acs.jpcb.8b00649

86. N. Sakashita, H.C. Watanabe, T. Ikeda, H. Ishikita, Structurally conserved channels in cyanobacterial and plant photosystem II, Photosynth. Res. 133 (2017) 75–85. https://doi.org/10.1007/s11120-017-0347-1

87. R.J. Debus, Alteration of the O_2-producing Mn_4Ca cluster in Photosystem II by the mutation of a metal ligand, Biochemistry 60 (2021) 3841–3855. https://doi.org/10.1021/acs.biochem.1c00504

88. M. Retegan, V. Krewald, F. Mamedov, F. Neese, W. Lubitz, N. Cox, D.A. Pantazis, A five-coordinate MnIV intermediate in biological water oxidation: Spectroscopic signature and a pivot mechanism for water binding, Chem. Sci.7 (2016) 72–84. https://doi.org/10.1039/C5SC03124A

89. R.J. Debus, Evidence from FTIR difference spectroscopy that D1-Asp61 influences the water reactions of the oxygen-evolving Mn_4CaO_5 cluster of photosystem II, Biochemistry 53 (2014) 2941–2955. https://doi.org/10.1021/bi500309f

90. I. Rivalta, M. Amin, S. Luber, S. Vassiliev, R. Pokhrel, Y. Umena, K. Kawakami, J-R. Shen, N. Kamiya, D. Bruce, G.W. Brudvig, M.R. Gunner, V.S. Batista, Structural-functional role of chloride in photosystem II, Biochemistry 50 (2011) 6312–6315. https://doi.org/10.1021/bi200685w

91. A. Boussac, A.W. Rutherford, M. Sugiura, Electron transfer pathways from the S_2-states to the S_3-states either after a Ca^{2+}/Sr^{2+} or a Cl^-/I^- exchange in Photosystem II from

Thermosynechococcus elongatus, Biochim. Biophys. Acta 1847 (2015) 576–586. https://doi.org/10.1016/j.bbabio.2015.03.006

92. S. Taguchi, T. Noguchi, H. Mino, Molecular structure of the S_2 state with a g=5 signal in the oxygen evolving complex of Photosystem II, J. Phys. Chem. B, 124 (2020) 5531–5537. https://doi.org/10.1021/acs.jpcb.0c02913

93. M. Amin, D. Kaur, M.R. Gunner, G. Brudvig, Toward understanding the S_2-S_3 transition in the Kok cycle of Photosystem II: Lessons from Sr-substituted structure, Inorg. Chem. Commun. 133 (2021) 108890. https://doi.org/10.1016/j.inoche.2021.108890

94. Y. Kato, T. Shibamoto, S. Yamamoto, T. Watanabe, N. Ishida, M. Sugiura, F. Rappaport, A. Boussac, Influence of the PsbA1/PsbA3, Ca^{2+}/Sr^{2+} and Cl^-/Br^- exchanges on the redox potential of the primary quinone Q_A in Photosystem II from *Thermosynechococcus elongatus* as revealed by spectroelectrochemistry, Biochim. Biophys. Acta 1817 (2012) 1998–2004. https://doi.org/10.1016/j.bbabio.2012.06.006

95. Y. Kato, A. Ohira, R. Nagao, T. Noguchi, Does the water-oxidizing Mn_4CaO_5 cluster regulate the redox potential of the primary quinone electron acceptor Q_A in photosystem II? A study by Fourier transform infrared spectroelectrochemistry, Biochim. Biophys. Acta 1860 (2019) 148082. https://doi.org/10.1016/j.bbabio.2019.148082

96. Y. Kato, H. Watanabe, T. Noguchi, ATR-FTIR spectroelectrochemical study on the mechanism of the pH dependence of the redox potential of the non-heme iron in Photosystem II, Biochemistry 60 (2021) 2170–2178. https://doi.org/10.1021/acs.biochem.1c00341
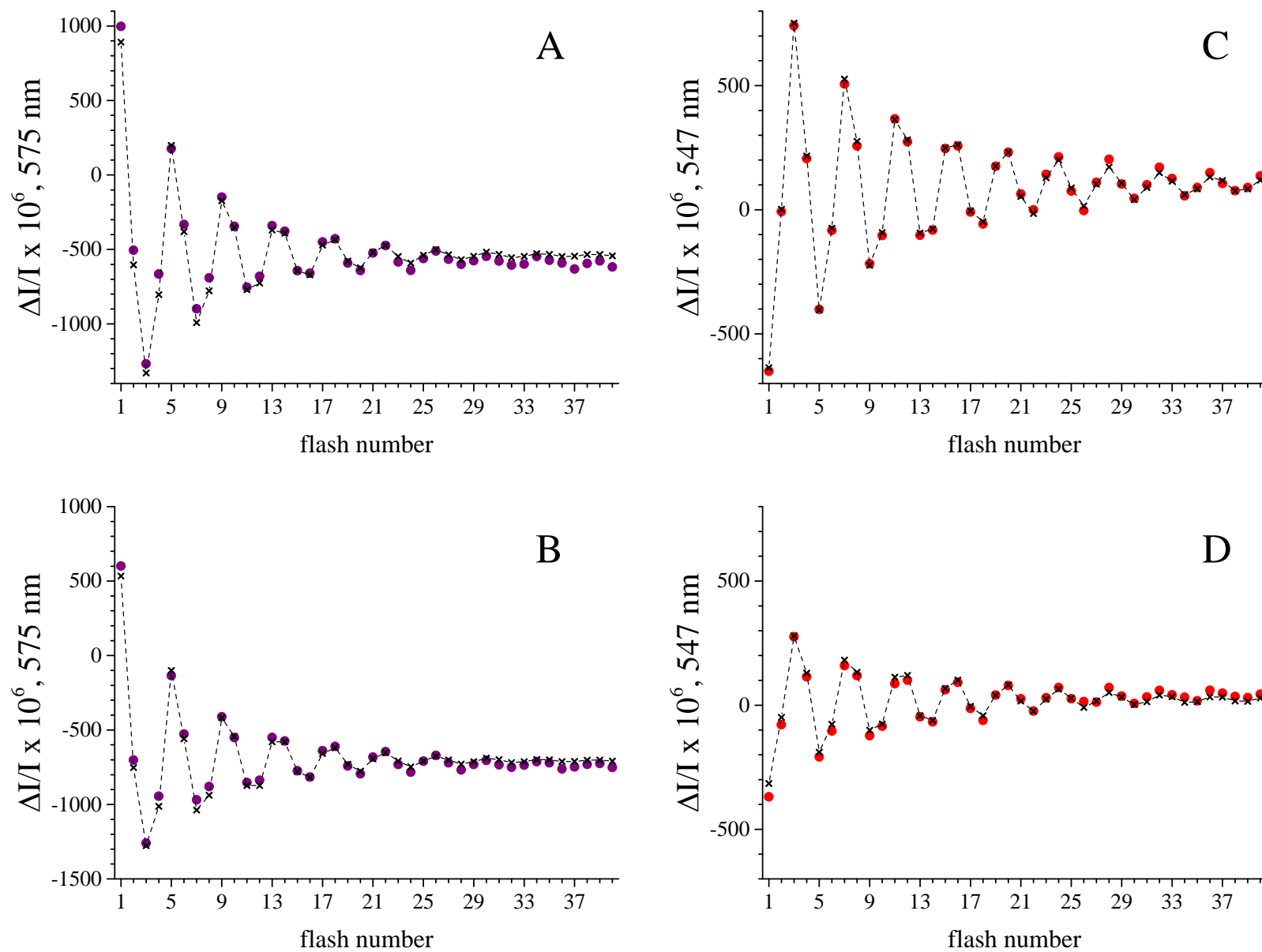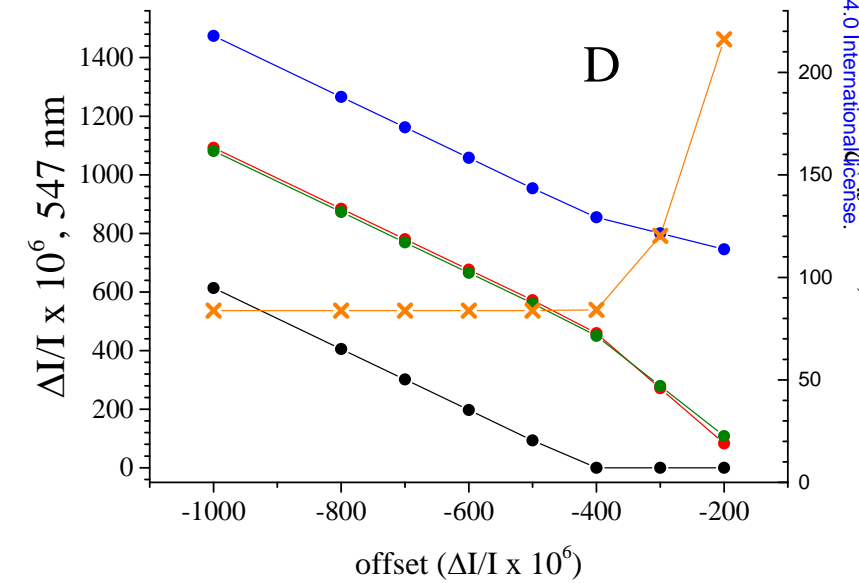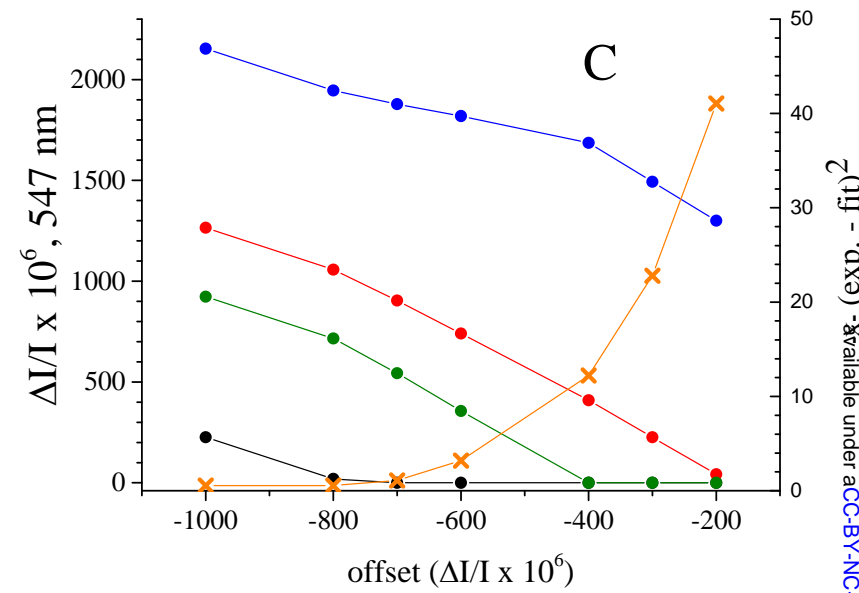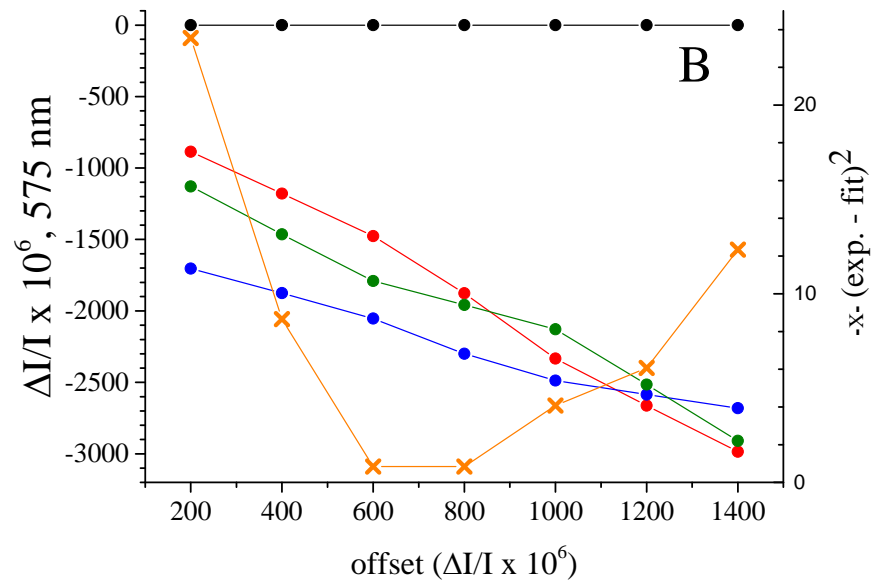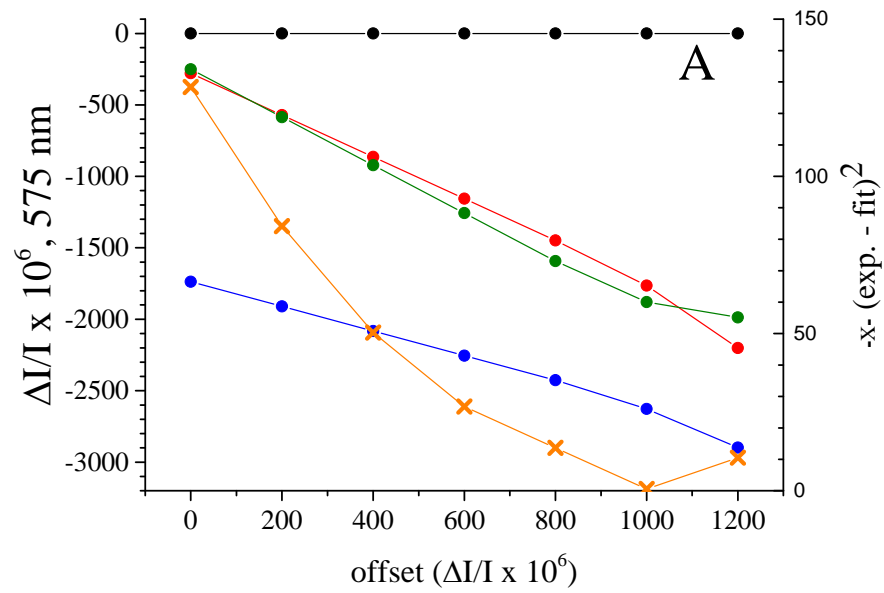
Fig. 1

Fig. 2

Fig. 3

Fig. 4

Fig. 5